Put a cork in it: Plugging the M2 viral ion channel to sink influenza

Pouria H. Jalily[a], Maggie C. Duncan[b], David Fedida[a], Jun Wang[c], Ian Tietjen[b,d,*]

[a] Department of Anesthesiology, Pharmacology, and Therapeutics, Faculty of Medicine, University of British Columbia, Vancouver, BC, Canada
[b] Faculty of Health Sciences, Simon Fraser University, Burnaby, BC, Canada
[c] Department of Pharmacology and Toxicology, College of Pharmacy, University of Arizona, Tuscon, AZ, USA
[d] The Wistar Institute, Philadelphia, PA, USA

ABSTRACT

The ongoing threat of seasonal and pandemic influenza to human health requires antivirals that can effectively supplement existing vaccination strategies. The M2 protein of influenza A virus (IAV) is a proton-gated, proton-selective ion channel that is required for virus replication and is an established antiviral target. While licensed adamantane-based M2 antivirals have been historically used, M2 mutations that confer major adamantane resistance are now so prevalent in circulating virus strains that these drugs are no longer recommended. Here we review the current understanding of IAV M2 structure and function, mechanisms of inhibition, the rise of drug resistance mutations, and ongoing efforts to develop new antivirals that target resistant forms of M2.

1. Introduction

Influenza A virus (IAV) is a significant and ongoing cause of human morbidity and mortality worldwide. While prophylactic vaccines can confer immunity against circulating virus strains, their effectiveness and extent of immunization coverage vary across populations from year to year. This variability contributed in part to the recent and notable 2017–2018 seasonal outbreak which is estimated by the Centers for Disease Control and Prevention to have caused approximately 710,000 hospitalizations and up to 79,400 deaths in the United States alone (CDC, 2018; Rolfes et al., 2019). Of particular concern are less common but historically regular pandemic outbreaks in populations with limited or no immunity that can result in hundreds of thousands to millions of deaths worldwide. Moreover, there still remains a significant technical gap to expedite a rapid vaccine production response, particularly in the face of an increasingly global spread of newly-emergent virus strains (Renaud et al., 2011; Hurt, 2014). Thus, additional countermeasures against IAV in the form of prophylactic and therapeutic antivirals continue to be needed.

The M2 protein is required for IAV replication and spread and is an established antiviral target. M2 is a proton-gated proton channel that belongs to a growing viroporin family of virus proteins. M2 ion channel activity is required for IAV replication, and adamantane-based M2 inhibitors including amantadine (**1**) and rimantadine (**2**; Fig. 1) were historically used as influenza antivirals. However, adamantane-resistant virus strains are now prevalent to the point that these drugs are

no longer recommended for therapeutic use (Bright et al., 2005; Deyde et al., 2007; Fiore et al., 2011; Hayden and De Jong, 2011). More than 95% of circulating adamantane-resistant viruses harbor a serine to asparagine mutation at amino acid position 31 in M2 (Ser31Asn; Bright et al., 2005), which distorts adamantane interactions within the pore without significantly affecting M2 ion channel activity or the fitness of viral replication (Balannik et al., 2010; Grambas et al., 1992; Pinto et al., 1992; Stouffer et al., 2008). Therefore, a major goal of current studies is to identify new inhibitors of adamantane-resistant M2.

Recent advances in molecular and structural biology, electrophysiology, and virology have produced crucial information about the basis of M2-based drug resistance. This in turn has shed light on novel drug development strategies and transitioning of those ideas to practical tools. Here we review the current state of IAV M2 viroporin research and ongoing efforts to identify and develop new antivirals against its drug-resistant forms.

2. The M2 viroporin of IAV

Viroporins are small (often ~60–120 amino acids), virally-encoded transmembrane proteins that regulate ion conduction across lipid membranes and are a frequent feature of both RNA and DNA viruses (Nieva et al., 2012; Nieto-Torres et al., 2015; Ouyang and Chou, 2014). Viroporins are frequently described as exhibiting a "channel-pore dualism," where some sequences are broadly permeable to ions and small molecules, while others are tightly-regulated channels that conduct

---

* Corresponding author. The Wistar Institute, Philadelphia, PA, USA.
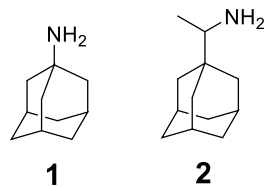 E-mail address: itietjen@wistar.org (I. Tietjen).

Fig. 1. The two FDA approved adamantanes amantadine (**1**) and rimantadine (**2**).

specific ions. Although the functions of most viroporins are not well understood, they are generally involved in conducting ions to facilitate viral entry, assembly, and/or release from host cells. Table 1 lists viroporins of representative viruses.

2.1. The role of M2 in IAV replication

The M2 protein of IAV is arguably the best understood viroporin. It consists of a 97 amino acid, type I transmembrane domain-containing protein which forms a tetrameric ion channel that is both proton-gated and proton-selective (Hong and DeGrado, 2012; Nieto-Torres et al., 2015). M2 is a multifunctional, modular protein where each segment performs one or more distinct function(s) (Wang et al., 2011c). Following viral entry, M2 expressed on the virion membrane transports protons from host cell endosomes to acidify the virion interior (Fig. 2). This low pH environment facilitates conformational changes in viral hemagglutinin (HA) and dissociation of viral ribonucleoprotein complex from M1 proteins to promote virion membrane fusion and release of viral RNA into the host cell. M2 proton gating function is, however, not required per se to convert HA into the membrane fusion competent state (Bui et al., 1996; Gutman et al., 1993; Martin and Heleniust, 1991). During viral egress, M2 also equilibrates the pH of trans-Golgi lumina and the cytoplasm, which may delay trafficking of virion particles and/or prevent HA from inappropriately adopting a low pH conformation (Alvarado-Facundo et al., 2015; Ciampor et al., 1992; Li et al., 2014; Pinto and Lamb, 2006; Sugrue et al., 1990). Compared to other influenza proteins, the sequence of M2 is highly conserved but has been shown to co-evolve with HA (Grambas et al., 1992; Rossman and Lamb, 2011). As such, M2's conductance rate closely correlates with HA's fusogenic propensity, where increased proton conductance by M2 correlates with more acid labile HA sequences (Grambas et al., 1992; Scholtissek et al., 1998). M2 has also been found to localize at the virus budding site on the host cell surface, where the amphipathic helix of M2 alters membrane curvature leading to membrane scission and release of new viral progeny (Chen et al., 2008; Rossman and Lamb, 2011; Rossman et al., 2010). Although protons are the preferred substrate, M2 can also act as a Na^+ and K^+ antiporter (Leiding et al., 2010). In particular, the ability of M2 to pass bulkier K^+ ions becomes

physiologically relevant in the endocytic pathway, where high Na^+ concentration in early endosome clusters is replaced by K^+ to allow for the subsequent release of the viral ribonucleoprotein bundle (Stauffer et al., 2014).

2.2. Regulation of ion conduction by M2

The existence of M2 was initially reported by Lamb et al., (1981) (Lamb et al., 1985, 1981; Lamb and Choppin, 1981; Lamb and Lai, 1981) Pinto et al. (1992) then demonstrated its ion channel activity in *Xenopus laevis* oocytes injected with M2 RNA and measured by the two-electrode voltage clamp (TEVC) method of electrophysiology, which has become the most common assay by far to measure M2 conductance and its inhibition by small molecules. However, several groups have used a variety of electrophysiological techniques including whole-cell patch-clamp of mammalian cells to probe the ion conduction properties of M2 (Chizhmakov et al., 1996; Holsinger et al., 1995, 1994; Jalily et al., 2016; Shimbo et al., 1996; Tu et al., 1996; Wang et al., 1995, 1993) For example, Chizhmakov et al. (1996) expressed M2 in mouse erythroleukemia cells and also observed selective conduction of protons.

Subsequent mutagenesis studies have further defined the specific M2 amino acid residues that are required for proton conduction and regulation (Fig. 3). Notably, a fragment of M2 encompassing the transmembrane domain and spanning as little as amino acids 21–51 was observed by TEVC to be sufficient to produce amantadine-sensitive, proton-dependent proton currents (Ma et al., 2009). To a first approximation, transmembrane mutations that are predicted to increase the pore radius (i.e., mutation to residues with smaller side chains) result in increased proton conduction, presumably either through the enhanced formation of water wires or transfer by His37 through conformational changes, while mutations to residues with bulkier side chains that reduce the pore radius also reduce conductance. For example, the introduction of Ala at Val27, which faces the extracellular and intraluminal surfaces and is thought to form the most constricted part of the channel, increases the pore entrance size and obliterates the N-terminal gating mechanism, thereby allowing for easier pore hydration and enhanced conduction (Balannik et al., 2010; Holsinger et al., 1994; Pielak and Chou, 2010). In contrast, introduction of bulky and/or hydrophobic residues such as Phe or Trp at Val27 results in non- or low-conducting M2 proteins. Similarly, mutations that reduce pore size at other locations including Ala30Trp, Ala30Pro, and Gly34Glu also slow the rate of proton conduction and frequently result in loss-of-function (Balannik et al., 2010).

Notably, a highly-conserved sequence of His37-XXX-Trp41 within the C-terminal end of the M2 transmembrane domain is regarded as the functional core of proton conductance (Pinto and Lamb, 2006; Tang et al., 2002; Venkatraman et al., 2005). Mutation of His37 to Gly or Gln

Table 1
Examples of viroporins from representative viruses.

| Virus Family	Virus	Viroporin(s)	Reference
Coronaviridae	SARS-CoV	E, 3a, 8a	Castaño-Rodriguez et al. (2018)
Flaviviridae	Hepatitis C virus	p7	Madan et al. (2015)
Orthomyxoviridae	IAV	M2	Pinto et al. (1992); To and Torres (2019)
	Influenza B virus		Mould et al. (2003)
	Influenza C virus		Pekosz and Lamb (1998)
	Influenza D virus		Kesinger et al. (2018)
Papillomaviridae	Papillomavirus 16	E5	Kabsch and Alonso (2002)
Phycodnaviridae	Paramecium bursaria chlorella virus 1	KcV	Thiel et al. (2011)
Picornaviridae	Poliovirus	2 B	Aldabe et al. (1996)
Pneumoviridae	Respiratory syncytial virus	Small hydrophobic (SH) protein	Gan et al. (2012)
Polyomaviridae	JC polyomavirus	Agnoprotein	Suzuki et al. (2010)
Reoviridae	Avian reovirus	p10	Bodelón et al. (2002)
Retroviridae	HIV-1	Vpu	Strebel (2014)
Rhabdoviridae	Bovine ephemeral fever virus	α1	Joubert et al. (2014)
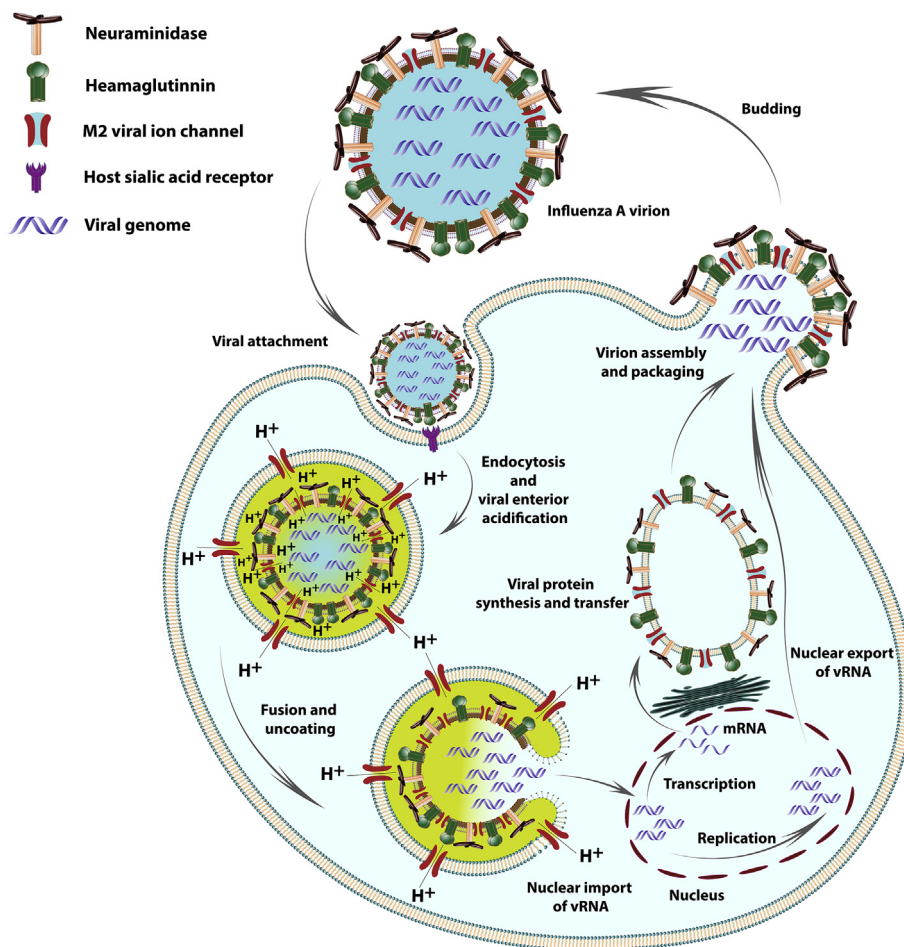
Fig. 2. Overview of IAV replication, with an emphasis on M2 functions. For clarity, only a subset of influenza proteins are shown.
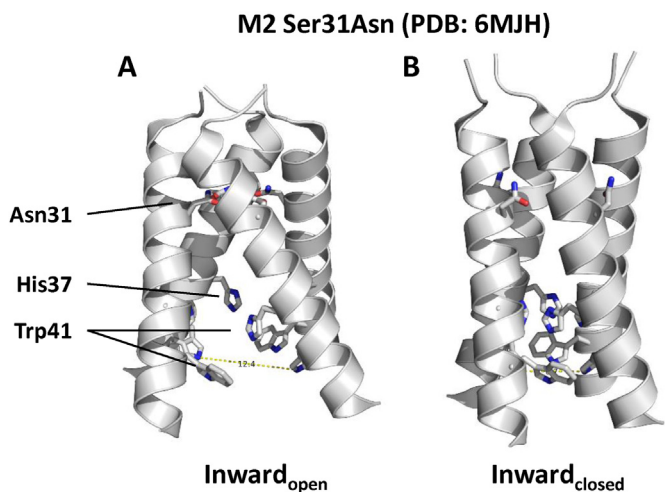
M2 Ser31Asn (PDB: 6MJH)

Fig. 3. X-ray crystal structures of M2-S31N (22–46) in the Inward$_{open}$ **(A)** and Inward$_{closed}$ **(B)** states (PDB: 6MJH (Thomaston et al., 2019);). In the Inward$_{open}$ state, the distance between the Trp41 indole nitrogen from opposition chains is 12.4 Å. In the Inward$_{closed}$ state, the distance between the Trp41 indole nitrogen from opposition chains is 6.7 Å.

results in enhanced conductance but also loss of proton selectivity and/or lack of pH dependence (Balannik et al., 2010; Wang et al., 1995). Moreover, mutation of Trp41 to Ala, Cys or Phe results in larger inward currents but also outward currents, indicating that Trp41 regulates unidirectional conductance (Balannik et al., 2010; Tang et al., 2002; Ma

et al., 2013). Another key residue, Ser31, is likely to face the pore interior, and its mutation to hydrophobic residues such as Ala negatively affects pore hydration, resulting in diminished conduction. At the other end of the His-Trp quartet, mutating Asp44 to hydrophobic residues such as Ala affects proton exit at the C-terminal end of the channel by increasing the energy barrier (Pielak et al., 2011). These and other mutations might also impact M2 function by indirectly affecting the inherent conduction moiety defined by the His37 tetrad or the gating mechanism defined by Trp41 (Gu et al., 2013; Ma et al., 2013).

2.3. The structure of M2

Recently reported structures of M2 have been instrumental toward understanding how adamantanes inhibit this ion channel and how drug resistance overcomes them, in addition to generally informing new M2 drug discovery and ion channel biology. Experimentally-determined protein structures derived from X-ray crystallography, solid-state and solution nuclear magnetic resonance (NMR), and protein-ligand complex structures originating from computational studies have also formed the basis of structure-based drug design. As of this writing, there were more than 35 structures of wild-type (WT) and drug-resistant A/M2 proteins available in the Protein Data Bank (PDB). Most of these were solved by X-ray techniques although some were elucidated using NMR.

While the mechanisms of proton shuttling that enable conduction remain incompletely understood, it is likely that experimental conditions such as pH, peptide length, lipid/detergent composition and thickness, and binding of small molecules affect the fundamental properties of M2 (Acharya et al., 2010; S. Cady et al., 2011; Du et al.,

2012; Kolokouris et al., 2019; Kovacs et al., 2000; Thomaston et al., 2013; Zhou and Cross, 2013). Among the available M2 structures in PDB, 2RLF and 3C9J were among the first structures solved using solution NMR and X-ray crystallography in micelles, respectively (Schnell and Chou, 2008; Stouffer et al., 2008). Hu et al. (2010) and Sharma et al. (2010) subsequently applied solid state NMR and molecular dynamics to explore the activation and conduction mechanisms of M2 at low pH (using PDB entries 2KQT, and 2L0J; Cady et al., 2010; Sharma et al., 2010). Although both studies support a "proton-relay" model of conduction, they differ with regard to the side-chain conformation of His37. The study by Hu et al. (2010) proposes a tightly-packed His37 tetrad which undergoes numerous reorientations and side chain rotations to relay protons. In contrast, the model by Sharma et al. (2010) suggests three distinct states for the His-Trp quartet: the "histidine-locked state", the "activated state", and the "conducting state", with transition between these states allowing for proton conductance. In this model, the "histidine locked state" exists when a proton is shared between two adjacent histidine residues (HisH$^+$-His) and the channel is locked in the non-conducting state. They further described the activation cascade at low extracellular pH, when a single hydronium ion approaches the non-protonated histidine in the HisH$^+$-His dimer, breaks this ionic bond, and transitions the channel to the "activated state", resulting in the formation of stable cation-p interactions between His37 and Trp41. The Trp41 tetrad forms a gate at the C-terminal end, and the perturbation of this cation-p interaction leads to conformational changes which in turn transition the quartet to the "conduction state". Here, protons are then donated to water molecules and relayed to the intracellular side (Fig. 4 and Sharma et al., 2010). The transition between these three steps requires small changes of the χ_2 angles of the His37 and Trp41 side chains. This contrasts with the model by Hu et al. (2010), where considerable reorientation of His37 and Trp41 residues are required to allow proton passage. Further experimental and theoretical data supporting both models are described in detail elsewhere (Hong and DeGrado, 2012; Thomaston et al., 2019; Watkins et al., 2019; Zhou and Cross, 2013).

3. Mechanisms of M2 inhibition by adamantanes

3.1. Advent of adamantanes as IAV M2 inhibitors

Ion channel activity of WT M2 is effectively antagonized by two FDA-approved adamantane-class drugs, amantadine (**1**) and rimantadine (**2**) (Fig. 1), in addition to numerous other adamantane and non-adamantane derivatives (Tables 2 and 3; Tataridis et al., 2007; Wang et al., 2013a; Wang et al., 2013b; Wu et al., 2014). During virus entry, amantadine's inhibition of M2 results in incomplete dissociation of M1 from ribonucleoprotein complexes, which in turn fail to enter the nucleus to initiate further replication. As M2 can also equilibrate pH

across the trans-Golgi network and the cytoplasm, amantadine-based M2 inhibition may also disrupt viral egress (Lamb, R.A. and Krug, 2001; Takeda et al., 2003).

Amantadine first obtained FDA approval in 1966 under the brand name "Symmetrel" for systemic use in humans for prophylaxis of Asian influenza (H2N2) (Davies et al., 1964; Schwab et al., 1969; Wingfield et al., 1969). However, during the first decade following its licensure, Symmetrel was not widely prescribed due in part to side effects such as agitation, confusion, and hallucinations (Keyser et al., 2000). Additionally, the molecular mechanism describing a direct link between amantadine and virus inhibition was not described until more than 25 years later (Duff and Ashley, 1992; Pinto et al., 1992). Rimantadine, sold under the brand name Flumadine, is a methylated derivative of amantadine which was licensed by FDA for the same indications in 1994.

3.2. Interactions of adamantanes with M2

Two pharmacologically relevant binding mechanisms were initially proposed for adamantanes (Fig. 5). In the first reported crystallographic structure of M2-bound amantadine at pH 5.3 (PDB: 3C9J), Stouffer et al. (2008) suggested that amantadine binds in a pocket located inside the intraluminal cavity and surrounded by the nonpolar side chains of Val27, Ala30, the C_β group of Ser31, and the C_α group of Gly34 (Fig. 5A). In this pore binding model, the authors proposed that amantadine, by entering the lumen of the channel, "plugs" the M2 pore and thus prevents the transport of protons. The model further suggests that Ser31Asn confers adamantane resistance by decreasing the pore size and occluding stable access of amantadine to the pore (Stouffer et al., 2008).

In a separate series of studies, an alternative but initially controversial binding mechanism for adamantanes, located external to the M2 pore, was also proposed (Pielak et al., 2009; Schnell and Chou, 2008, Fig. 5B). In these studies, rimantadine was found to bind to Asp44 on the C-terminal, lipid-facing side of the helices. The solution NMR structure (PDB: 2RLF), solved at pH 7.5, showed an allosteric mechanism of inhibition where four drug molecules were proposed to stabilize the inactivated state of M2, thereby preventing proton-gated M2 opening and proton transfer. In this binding mechanism, perturbation of the extra-luminal drug binding pocket as a result of Ser31Asn mutation rendered rimantadine incapable of effectively binding to the allosteric site (Pielak et al., 2009).

To reconcile these findings, a series of both experimental and computational studies were rapidly reported (Jing et al., 2008; Balannik et al., 2009; Cady et al., 2010; Carpenter et al., 2008; Chuang et al., 2009; Stouffer et al., 2008). Jing et al. (2008) demonstrated that the intraluminal binding site is more physiologically relevant through conducting whole-cell electrophysiology and antiviral assays using
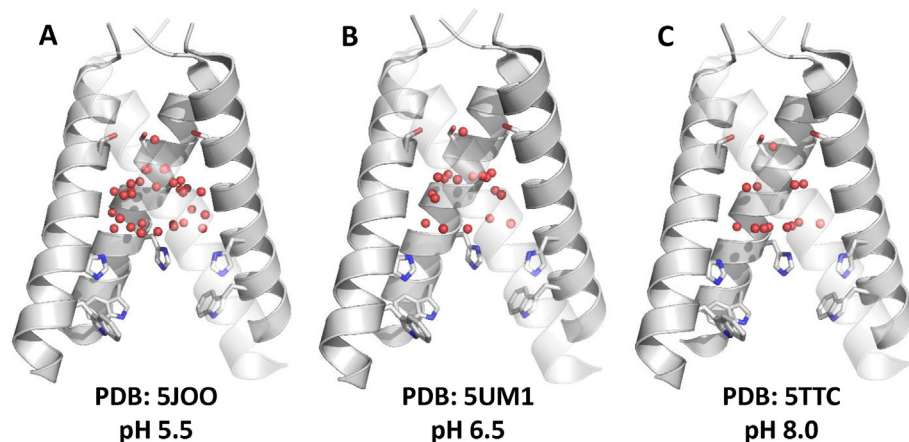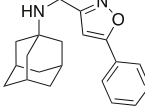

Fig. 4. Water molecules in the wild-type M2 proton channel at different pH conditions. The structures were determined by X-ray free-electron laser (XFEL) at room temperature. **(A)** Low pH (5.5) structure (PDB: 5JOO). **(B)** Intermediate pH (6.5) structure (PDB: 5UM1). **(C)** High pH (8.0) structure (PDB: 5TTC). Waters are shown as spheres (Thomaston et al., 2017).

A

PDB: 5JOO
pH 5.5

B

PDB: 5UM1
pH 6.5

C

PDB: 5TTC
pH 8.0

Table 2
Examples of adamantane-based inhibitors of drug-resistant M2. NR, not reported.

Compound	Name	Structure	Activity				Reference
			Assay	IC_{50}/EC_{50}	Virus Strain	MDCK cell toxicity (CC_{50})	
1	Amantadine		TEVC	WT: 16 μM V27A: > 500 μM S31N: 200 μM	A/Udorn/72	> 100 μM (multiple reports)	Wang et al. (2013a)
			PRA	WT: 0.3 μM S31N: 22 μM	A/WSN/33		
2	Rimantadine		TEVC	WT: 11 μM S31N: > 2 mM	A/Udorn/72	> 100 μM (multiple reports)	
3	M2WJ352		TEVC PRA	S31N: 14 μM S31N: 14 μM	A/Udorn/72 A/WSN/33	NR	
4	M2WJ332		TEVC PRA	S31N: 16 μM S31N: 0.1 μM	A/Udorn/72 A/WSN/33	100 μM (Li et al., 2016a)	
5	M2WJ379		TEVC PRA	S31N: 16 μM S31N: 1 μM	A/Udorn/72 A/WSN/33	NR	
6			TEVC	S31N: 74.4% inhibition at 100 μM WT: 12.0% inhibition at 100 μM	A/Udorn/72	33.9 μM	Li et al. (2016a, 2016b)
			PRA	S31N: 1.7 μM	A/WSN/33		
7	Benzdiol		TEVC	WT: 60 μM S31N: 35 μM	A/Udorn/72	NR	Wang et al. (2013b)
			PRA	WT: complete inhibition at 1 μM S31N: 3.2 μM	A/WSN/33		
8	BC035		TEVC	WT: 77% inhibition at 100 μM S31N: 76% inhibition at 100 μM	A/Udorn/72	123 μM	Wu et al. (2014)
			PRA	WT: 4.6 μM S31N: 1.8 μM	A/WSN/33		
9	Spirane-adamantane amine		TEVC	WT: 18 μM L26F: 6 μM V27A: 0.3 μM	A/Udorn/72	27.6 μM	Hu et al. (2017a); Wang et al. (2011a)
			PRA	WT: 0.3 μM N31S + V27A: 1.8 μM	A/Udorn/72 A/WSN/33		
10	Spirane-adamantane dithiane		TEVC	WT: 64% inhibition at 100 μM V27A: 0.4 μM	A/Udorn/72	74.8 μM	Hu et al. (2017a)
			PRA	WT: 0.07 μM N31S + V27A: 1.0 μM	A/WSN/33		
11	Organosilane		TEVC	WT: 9% inhibition at 100 μM S31N: 86% inhibition at 100 μM	A/Udorn/72	40.7 μM	Hu et al. (2017b)
			PRA	S31N: 0.4 μM	A/WSN/33		
12			TEVC	WT: 4.1 μM V27A: 3.6 μM	A/Udorn/72	> 100 μM	Barniol-Xicota et al. (2017)
			PRA	WT: 0.14 μM	A/HK/7/87		
13			TEVC	WT: 1.9 μM V27A: 16.2 μM	A/Udorn/72	10 μM	
			PRA	WT: > 50 μM	A/HK/7/87		
14			TEVC	S31N: 75.5% inhibition at 100 μM	A/CA/07/2009	59.3 μM	Li et al. (2017); Musharrafieh et al. (2018)
			PRA	S31N: 1.2 μM S31N + V27A: 23.7 μM			
15			TEVC	S31N: 84.3% inhibition at 100 μM	A/CA/07/2009	146.6 μM	Musharrafieh et al. (2018); Wang et al. (2018)
			PRA	S31N: 0.3 μM			
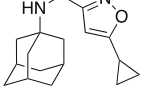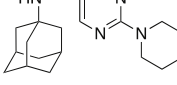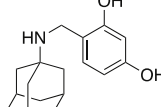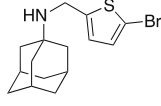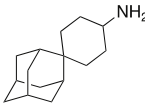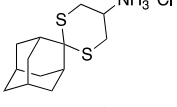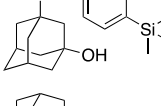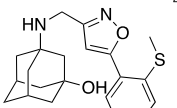
Table 2 (*continued*)

Compound	Name	Structure	Activity				Reference
			Assay	IC$_{50}$/EC$_{50}$	Virus Strain	MDCK cell toxicity (CC$_{50}$)	
16			TEVC	S31N: 47.9% inhibition at 100 μM	A/WSN/33	> 300 μM	Wang et al. (2018)
			PRA	S31N: 0.5 μM			
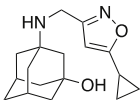
mutant and chimeric M2 forms. By mutating the critical Asp44 residue to alanine, Jing and coworkers continued to observe inhibition by amantadine in both electrophysiological and antiviral plaque assays, suggesting that the allosteric-binding site is not pharmacologically essential (Jing et al., 2008). Additionally, in a chimeric ion channel based on the M2 of influenza B, which is normally amantadine-insensitive due to a larger and more hydrophilic transmembrane pore (Mould et al., 2003), substitution with the M2 transmembrane domain from influenza A restored amantadine sensitivity (Jing et al., 2008). Using solid-state NMR, Cady et al. (2010) also reported that the channel pore was the preferred binding site (PDB: 2KQT), where amantadine preferentially localized to a hydrophobic cage formed by Ala30, Ser31, and Gly34. Hydrophobic interactions between Val27 side chains and the adamantane cage were also observed, and the ammonium group of amantadine showed hydrogen bonding to water molecules and pore-facing residues that stabilized its interactions in the occluded pore. The authors also reported that interactions with the allosteric binding site were observed only at high amantadine concentrations and were thus less probable as the primary mode of M2 inhibition. In further support of the pore-binding model, mutation of Asp44, proposed as the key residue of the allosteric binding mechanism, to six different amino acids (Asp44Ala, Asp44Lys, Asp44Asn, Asp44Phe, Asp44Gly, and Asp44Thr) did not affect inhibition by amantadine (Balannik et al., 2010). Notably, in further testing their initial hypothesis of an allosteric binding site of amantadine to M2, Pielak et al. (2011) next generated an M2 chimera where the C-terminus was derived from the amantadine-insensitive M2 of influenza B virus (PDB: 2LJB). Contrary to their previously proposed allosteric binding mechanism, using solution NMR, they described the rimantadine binding pocket to be preserved within the pore of the chimeric M2 protein. In a series of surface plasmon resonance experiments, the pore-binding site was also found to be more energetically favorable than the allosteric binding site, although the latter did remain sensitive to amantadine (Rosenberg and Casarotto, 2010).

Another computational study using small molecular probes and solvent mapping techniques found the pore-binding site to be more energetically favored, although the allosteric site was also observed under some conditions (Chuang et al., 2009). Gu et al. (2011) also applied molecular dynamics approaches to study the antagonistic effects of known M2 inhibitors and observed that, while interactions with the pore-binding site were more thermodynamically stable, ligands bound slowly and poorly dissociated due to a high energy barrier of binding. In contrast, the allosteric binding was readily accessible, the energy barrier for binding was minimal, and drug binding was less stable and more readily dissociated. Moreover, the initial NMR structure (PDB: 2RLF) did not show evidence of an intraluminal binding site but rather binding at the allosteric peripheral site in the lipid interface. However, this can also be interpreted by noting that the NMR structure was narrower as compared to the counterpart X-ray structure (PDB: 3C9J) due to a smaller tilt angle which resulted in transmembrane helices being overly parallel. This finding further alerted the field to the importance of the protein crystallization environment and emphasised the risk of crystal packing distortions across all published crystal structures (Cross et al., 2012).

Later, through synthesizing organosilane probes and measuring

intermolecular NOESY spectra in DPC micelles, Wang et al. (2011a) also mapped the drug binding site at the N-terminal lumen of A/M2 near Val27. Recent high-resolution X-ray crystal structures of M2 in complex with adamantanes and other M2 channel blockers published by DeGrado lab also unambiguously recognized the intra-luminal binding site (Thomaston et al., 2018, 2019). Taken together, these follow-up studies support that amantadine inhibits IAV M2 by plugging the pore (Fig. 5A).
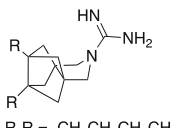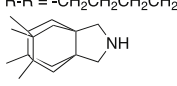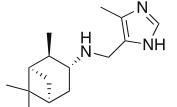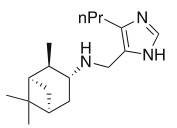
More recently, the binding affinities of the R and S enantiomers of rimantadine to M2 have also been questioned. Surprisingly, by comparing the isotropic chemical shift changes of rimantadine's two enantiomers through ssNMR experiments and molecular dynamics simulations, Wright et al. (2016) proposed that the 2-R enantiomer may bind to full-length M2 differently and with a higher affinity relative to the 2-S enantiomer. However, a subsequent series of *in vitro* and cellular assays, electrophysiology experiments, and molecular dynamics simulations indicated that both enantiomers exhibited similar channel blockade in TEVC experiments, comparable antiviral activity in plaque assays, and similar free energies of binding in isothermal titration calorimetry and computational simulations (Drakopoulos et al., 2017). The latter observations are also consistent with experimental data showing similar efficacy of these two enantiomers in mice (Aldrich et al., 1971).

3.3. The rise of drug-resistant M2

In addition to Ser31Asn (and further consistent with the pore-binding model described above), the mutations Leu26Phe, Val27Ala, Ala30Thr and Gly34Glu also confer adamantane resistance (Bright et al., 2006; Cady et al., 2009a, 2009b). Large-scale sequence analyses of circulating IAV strains indicate that Leu26Phe, Val27Ala and Ser31Asn are the three major adamantane-resistance mutations found in transmissible viruses (Furuse et al., 2009a, 2009b). Among these, Ser31Asn is the prevalent mutation in more than 95% of adamantane-resistant strains (Dong et al., 2015; Nelson et al., 2009), although a recent study reported a potential rise in the frequency of virus strains containing the Val27Ala and Ser31Asn double mutations (Durrant et al., 2014). A recent crystallography study reported that elimination of hydrophobic contacts that are essential for adamantane drug binding is the underlying cause behind adamantane resistance to Val27Ala mutant (Thomaston et al., 2020). In contrast to the Val27Ala single mutation that results in complete resistance to amantadine, M2 sequences containing Ser31Asn can still be inhibited by amantadine *in vitro*, albeit with approximately 200-fold higher concentrations in TEVC experiments and plaque reduction assays (PRAs) and substantiall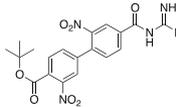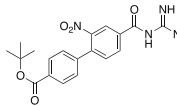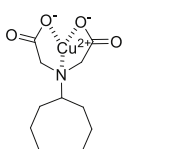y higher than what is therapeutically-achievable (Wang et al., 2013a). Notably, the Ser31Asn mutation has been isolated in curated virus strains that were in circulation before use of adamantanes, and so the prevalence of the Ser31Asn mutation in the wild may not be exclusively the result of drug selection pressure. This contrasts with mutations such as Val27Ala which appear more likely than Ser31Asn to have evolved as a result of drug selection pressure (Furuse et al., 2009a, 2009b).

The effects of the Ser31Asn mutation on M2 pore size and proton conduction have been elucidated in exquisite detail. For example, the

Table 3
Examples of non-adamantane-based inhibitors of drug-resistant M2. NR, not reported.

Compound	Name	Structure	Activity				Reference
			Assay	IC$_{50}$/EC$_{50}$	Virus Strain	MDCK cell toxicity (CC$_{50}$)	
17	Polycyclic pyrrolidine	R-R = -CH$_2$CH$_2$CH$_2$CH$_2$-	TEVC	WT: 3 μM V27A: 0.3 μM	A/Udorn/72	10 μM	Rey-Carrizo et al. (2013)
			CPE	WT: 0.37 μM	A/HK/7/87		
18	Polycyclic amine		TEVC	WT: 18 μM L26F: 8.6 μM V27A: 0.7 μM	A/Udorn/72	49 μM	Rey-Carrizo et al. (2014)
			PRA	V27T + S31N: 1.8 μM	A/PR/8/34		
19	Pinanamine derivatives		TEVC	WT: 95% inhibition at 100 μM S31N: 27% inhibition at 100 μM	A/Udorn/72	251.5 μM	Dong et al. (2015); Zhao et al. (2012)
			CPE	WT: 3.2 μM S31N: 95.5 μM	A/HK/68 A/WSN/33		
20			TEVC	WT: 98% inhibition at 100 μM S31N: 3.5% inhibition at 100 μM	A/Udorn/72	200.2 μM	Dong et al. (2016)
			CPE	WT: 2.5 μM S31N: 3.4 μM	A/HK/68 A/WSN/33		
21	Spiranamine		TEVC	WT: 12.6 μM V27A: 85 μM	A/Udorn/72	NR	Balannik et al. (2009)
22	Silaspirane derivative		TEVC	WT: 13.7 μM V27A: 31.3 μM	A/Udorn/72	NR	Wang et al. (2011b)
23	Hexamethylene amiloride		SEVC	WT: 1.3 μM S31N: 10% inhibition at 100 μM	A/HK/1073/99	4.7 μM	Balgi et al. (2013); Jalily et al. (2016)
24	Acylguanidine derivatives		SEVC	WT: 0.2 μM	A/HK/1073/99	> 100 μM	Jalily et al. (2016)
			PRA	WT: 2.3 μM	A/PR/8/34		
25			SEVC	WT: 0.6 μM S31N: 4.4 μM	A/HK/1073/99	55 μM	
			PRA	WT: 40 μM S31N: 18 μM	A/PR/8/34		
26			SEVC	WT: 20% inhibition at 100 μM S31N: 42 μM	A/HK/1073/99	25 μM	
			PRA	WT: 6.9 μM S31N: 1.5 μM	A/PR/8/34		
27	Divalent copper complex		TEVC	S31N: 90% inhibition at 100 μM	A/Udorn/72	147 μM	Gordon et al. (2017)
			PRA	WT: 3.7 μM	A/Victoria/03/75		
				S31N: 0.7 μM S31N: 2.1 μM	A/CA/07/09 A/WSN/33		
28	Salinomycin		Virus-like particle conductance assay	WT 54% inhibition at 100 μM S31N: 72% inhibition at 100 μM M2 from influenza B: ~60% at 100 μM	A/PR/8/34 B/Lee/40.	35.6 μM	Jang et al. (2018)
			CPE	S31N: 0.7 μM S31N: 1.9 μM	A/PR/8/34 A/CA/07/09		
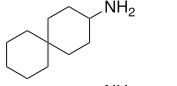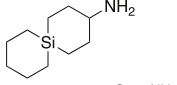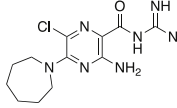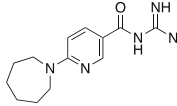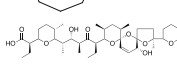
solution NMR structure (PDB: 2RLF; Schnell and Chou, 2008) presents Ser31 between two alpha-helices, and its mutation to the larger asparagine expands the pore by creating a kink in each monomer which would be expected to result in higher conductance. In contrast, the crystal structure (PDB: 3C9J; Stouffer et al., 2008) shows Ser31 facing the pore, where mutation to asparagine decreases the pore size and would be expected to reduce conductance. However, Holsinger et al. (1994) did not observe a difference in the rate of proton conduction due to the Ser31Asn mutation as measured by single electrode electrophysiology recordings. This result was further confirmed by Balannik et al. (2010) in two-electrode voltage clamp assay in which S31N mutant had indistinguishable specific conductance as M2 WT. Regardless,
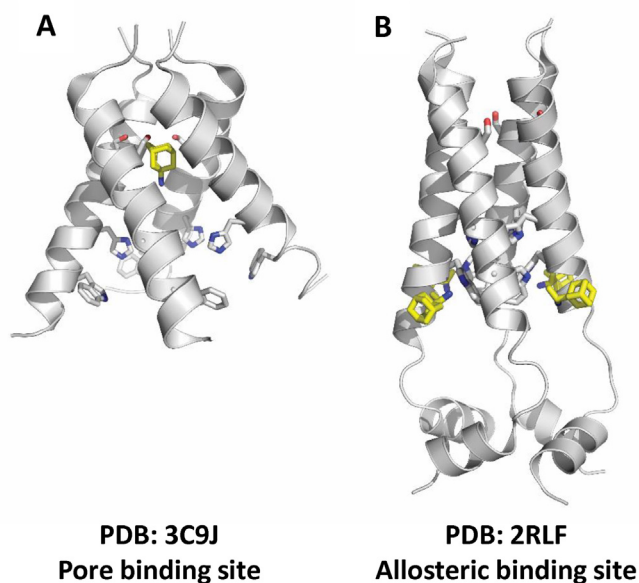
Fig. 5. Drug binding site controversy of the IAV M2 proton channel. **(A)** X-ray crystal structure of M2 (22–46) (PDB: 3C9J). **(B)** Solution NMR structure of M2 (18–60) (PDB: 2RLF).

being located at a pore lining residue, the Ser31Asn mutation is likely to alter the diameter as well as the polarity and dynamics of the channel pore, resulting in changes between the observed interactions of the Ser31Asn channel and amantadine when compared to WT M2 (Gleed et al., 2015). Interestingly, in the solved X-ray crystal structure for M2 containing the Ser31Asn mutation (PDB: 5C02; (Thomaston and DeGrado, 2016; Thomaston et al., 2018, 2019), in the absence of a drug molecule in the pore and in the Inward_open state, Asn31 was found to face the pore and was stabilized by H-bonds formed with the carbonyl groups of neighboring Asn31 (Fig. 3A). This arrangement sterically constricts the adamantane binding site in the pore. In contrast, in the Inward_closed state, Asn31 was tucked away from the centre of the pore and stabilized by forming H-bonds with carbonyls at the monomer-monomer interface, thereby twisting the helices and narrowing the pore near the binding site (Fig. 3B). Alternatively, using a solution NMR structure Wang et al. (2013) demonstrated that the Asn31 carboxamide could be stabilized in a pore-facing conformation through a bidentate

interaction with the M2-S31N inhibitor M2WJ332 (compound **4**; Table 2; Fig. 6B). These observations further emphasize that the orientation of Asn31 in the pore is dependent on the conformational state of the protein and/or the presence of interacting drug molecule in the lumen of the pore.

4. Development of inhibitors to drug-resistant M2

An extensive combination of molecular dynamics simulations (Khurana et al., 2011; Wang et al., 2011a), X-ray crystallography (Acharya et al., 2010; Stouffer et al., 2008), and NMR spectroscopy (Cady et al., 2011; Wang et al., 2009, 2011a, 2013a) along with iterative cycles of medicinal chemistry, electrophysiological testing, and antiviral assaying have led to the discovery of several classes of compounds that inhibit at least one of the three major drug-resistant mutations (Leu26Phe, Val27Ala, or Ser31Asn) with efficacies comparable or better than amantadine against WT M2. While several other compounds are reported throughout the literature to inhibit M2 Ser31Asn-containing viruses, the mechanism of action of many of them is not confirmed to be mediated through M2 as many of these compounds were not tested in M2-specific assays. The most promising compounds have therefore been validated by both antiviral *and* M2 conductance assays, the vast majority of which have been assessed by TEVC. These "second-generation" inhibitors of drug-resistant M2 can be broadly categorized in two main groups: adamantanes (Table 2) and a series of chemically diverse non-adamantane molecules (Table 3). While numerous compounds are reported by many groups, in addition to those cited in Tables 2 and 3, we have highlighted particular compounds with electrophysiology-based IC$_{50}$s and PRA-based EC$_{50}$s at low or sub-micromolar concentrations, which approximate the activities of amantadine and rimantadine in these assays with wild-type M2. Clearly, the efficacy of a given inhibitor as measured by TEVC and PRA does not necessarily translate to efficacy *in vivo*. However, a subset of these inhibitors has recently advanced to preclinical and animal efficacy studies, where promising results are reported. Additional compounds that inhibit WT M2, in addition to early but weaker inhibitors of M2 Val27Ala and Ser31Asn, have been reviewed elsewhere (Duque et al., 2011; Wang et al., 2015).

4.1. Adamantane-based inhibitors

Among the many molecules synthesized and tested by the DeGrado group, compounds **3** and **4** emerged as the first promising candidates of
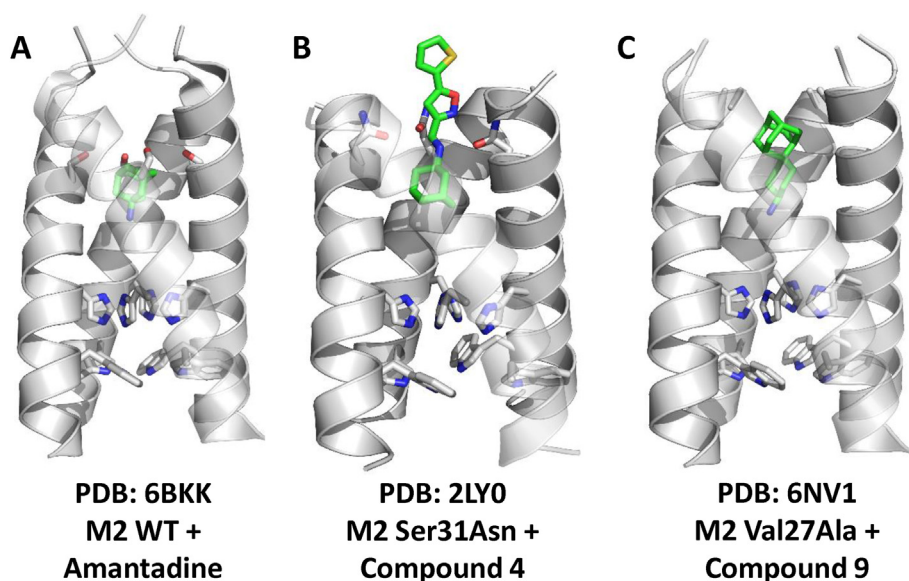
Fig. 6. Structures of M2 in complex with channel blockers. **(A)** X-ray crystal structure of M2-WT (22–46) in complex with amantadine (**1**) (PDB: 6BKK; Thomaston et al., 2018). **(B)** Solution NMR structure of M2-S31N (19–49) in complex with (**4**) (PDB: 2LY0 (Wang et al., 2013);). **(C)** X-ray crystal structure of M2-V27A (22–46) in complex with spiro-adamantyl amine (**9**) (PDB: 6NV1; Thomaston et al., 2020).

PDB: 6BKK
M2 WT +
Amantadine

PDB: 2LY0
M2 Ser31Asn +
Compound 4

PDB: 6NV1
M2 Val27Ala +
Compound 9

M2 Ser31Asn inhibition. TEVC experiments revealed 50% inhibitory concentration (IC_{50}) values of 14 and 16 μM for **3** and **4**, respectively, against the Ser31Asn form of M2, which was comparable to amantadine's inhibition of WT M2 in the authors' hands (16 μM; Wang et al., 2013a). Moreover, compound **4** bound to Ser31Asn M2 with such high affinity that structure determination by solution NMR was possible. In their structure model (PDB: 2LY0), **4** was found to be clamped between the side chains of three Asn31 residues while having its amine group pointing towards the M2 N-terminus (Fig. 6B). The adamantane cage fit within the hydrophobic pocket between Asn31 and Gly34, and the positively charged ammonium group of the adamantane formed hydrogen bonds via water molecules with two asparagines, while the third asparagine and the nitrogen of isoxazole of **4** formed a bidentate interaction. The side-chain carbonyl of Asn received a hydrogen bond from the ammonium group, and the carboxamide of the same Asn donated a hydrogen bond to the endocyclic nitrogen of isoxazole. On the other end of compound **5**, the thiophene moiety sit against four methyl groups of Val27 and was stabilized by hydrophobic interactions. Notably, this distal hydrophobic group could be substituted by other similar moieties such as benzene (**3**) and cyclopropane (**5**) without substantially compromising efficacy. Molecular dynamics experiments also supported the potential drug-protein interactions observed in NMR experiments. Numerous additional inhibitors of M2 Ser31Asn have since been reported by the DeGrado and Wang laboratories: for example, compound **6** inhibited 74.4% of M2 Ser31Asn activity by TEVC and virus replication with a 50% effective concentration (EC_{50}) of 1.7 μM (Li et al., 2016a, 2016b; 2017) in PRA. Notably, compound **6** also inhibited 12% of WT M2 channel activity by TEVC at 100 μM (Li et al., 2016a).

Additional adamantane-based compounds have also been reported to inhibit multiple forms of M2. For example, Wang et al. (2013b) proposed that installation of aromatic groups to the amine group of amantadine might also improve inhibitory activity against Ser31Asn M2 while maintaining activity against WT M2. This design hypothesis lead to the synthesis and discovery of benzyl-substituted amantadine derivatives, among which a benzdiol (**7**) was reported as the first potent WT and Ser31Asn M2 dual-inhibitor with IC_{50} values of 60 and 35 μM, respectively, as measured by TEVC. By plaque reduction assay, **7** further showed a EC_{50} of 3.2 μM against the A/WSN/33 M2 Ser31Asn strain of IAV and complete inhibition of WT (Ser31 M2-containing) virus at 1 μM. Another series of dual inhibitors, exemplified by compound **8**, inhibited 77 and 76% of currents from both M2 WT and Ser31Asn, respectively, as measured by TEVC. Compound **8** additionally inhibited amantadine sensitive and resistant viruses with EC_{50} values of 4.6 and 1.8 μM, respectively, as measured by PRA.

Wang et al. (2011a) also reported design of a spirane-adamantane derivative (**9**; Fig. 6C) that inhibited WT (IC_{50} = 18 μM), Leu26Phe (IC_{50} = 6 μM), and Val27Ala (IC_{50} = 0.3 μM) forms of M2, as measured by TEVC, which in turn were comparable to amantadine's activity against WT channel in this study (IC_{50} of 15.7 μM). Additionally, based on their previous findings in identifying a dual inhibitor of WT and Val27Ala M2 (**10**), Hu et al. (2017b) designed and reported the first class of organosilanes that exhibited potent antiviral activity against amantadine-resistant and oseltamivir-resistant viruses. Their most potent organosilane (**11**) was able to inhibit M2 Ser31Asn currents in TEVC experiments by ~86% at 100 μM and inhibited an A/WSN/33 (H1N1) virus encoding M2 Ser31Asn with an IC_{50} of 0.4 μM (Hu et al., 2017b). Barniol-Xicota et al. (2017) also reported a series of dual M2 WT and Val27Ala inhibitors. However, while both compounds **12** and **13** were potent inhibitors of both the WT M2 and M2 Val27Ala, with IC_{50}s ranging from 1.9 to 16.2 μM by TEVC, only **12** exhibited any antiviral activity (EC_{50} = 0.14 μM; Barniol-Xicota et al., 2017), while **13** also exhibited toxicity in MDCK cells (50% cytotoxic concentration (CC_{50}) = 10 μM). The authors proposed that the antiviral activity of these dual inhibitors is highly dependent on "slow and steady" binding of inhibitors, where a k_d of 10^{-6} or less is needed to be observed by TEVC.

An important question is whether these second-generation inhibitors are capable of giving rise to additional drug-resistant forms of M2 and influenza viruses with comparable replicative fitness. In beginning to address this, the Wang group first reported that *in vitro* passaging of influenza virus in the presence of increasing concentrations of the M2 Ser31Asn inhibitor **5** resulted in a novel M2 mutation, Leu26Ile, which conferred drug resistance. This mutation was also co-observed with an occasional Asn31Ser mutation which reverted back to Asn31 upon drug withdrawal. In contrast, passaging with the dual inhibitor compound **8** resulted in Asn31Asp and Ile32Thr mutations which also reverted after drug withdrawal (Ma et al., 2016). Both sets of mutations were confirmed to be resistant to their respective selecting drugs by TEVC.

The Wang group have also reported results from *in vitro* passaging of two M2-S31N inhibitors **14** and **15**, which potently inhibited both M2 current activity by TEVC (75.5 and 84.3% at 100 μM) and adamantane-resistant viruses (EC_{50}s = 1.2 and 0.3 μM, respectively; Li et al., 2017; Wang et al., 2018; Musharrafieh et al., 2018). Remarkably, unlike amantadine, which readily gave rise to resistance after a single passage *in vitro*, compounds **14** and **15** required 4–5 passages before two resistance mutations (Val27Ile and Leu26Ile respectively) were detected *in vitro*, suggesting a higher genetic barrier to resistance. Interestingly, reversion of M2 back to Ser31 was not observed. Further passaging of Ser31Asn + Leu26Ile virus with **15** at higher concentrations selected for a third Ala30Thr. Notably, while both M2 and viruses containing Ser31Asn + Val27Ile or Leu26Ile exhibited similar proton conductance properties and viral replication fitness relative to the single Ser31Asn mutant, the addition of Ala30Thr to Ser31Asn and Leu26Ile resulted in substantially reduced M2 proton conductance and viral replication. These observations may suggest that the viable evolutionary space of M2 in response to selection with these compounds may be limited.

In further M2 resistance studies, Compound **16** was also reported as a potent inhibitor of both M2 Ser31Asn by TEVC (47.9% inhibition at 100 μM, although its proposed slow-binding kinetics may underestimate its efficacy) and *in vitro* virus replication (EC_{50} as low as 0.2 μM; Wang et al., 2018) Serial passaging of virus in the presence of increasing concentrations of **16** resulted in a novel and unexpected drug-resistance mutation, Leu46Pro, positioned at the distal end of the M2 transmembrane helix. Interestingly, Leu46Pro did not significantly change proton conductance or amantadine sensitivity on its own in WT M2. However, in the presence of Ser31Asn, the Leu46Pro mutation rendered compounds **14–16** ineffective in TEVC experiments. Through molecular modelling and molecular dynamics simulations, the authors proposed that Leu46Pro, despite being located outside of the canonical M2 binding sites of adamantanes, could affect the size of the M2 pore where compounds **14–16** were proposed to interact (Musharrafieh et al., 2019). Taken together, these results suggest that when compared to amantadine and WT M2, the genetic barrier for drug resistance is likely to be higher for adamantane-derived compounds that target M2 Ser31Asn, at least *in vitro*.

The preclinical and *in vivo* potential of M2 Ser31Asn-inhibiting adamantane derivatives are now beginning to be elucidated. For example, Compounds **5**, **8**, **10**, and **16** have been reported to inhibited virus strains with resistance to the licensed neuramindase inhibitor oseltamivir (Hu et al., 2017a; Ma et al., 2016; Wang et al., 2018). In oseltamivir-sensitive viruses, **5** and **16** also synergized with oseltamivir, raising the possibility of combination therapies where lower doses of drugs can be used to minimize the risk of toxicities without sacrificing antiviral efficacy (Ma et al., 2016; Wang et al., 2018). Compound **16** also exhibited favorable *in vitro* pharmacokinetic properties such as half-life of at least 145 min in mouse and human liver microsome stability assays. It also exhibited good cellular permeability in Caco-2 cells ($\sim28 \times 10^{-6}$ cm/s) and did not inhibit a panel of five CYP enzymes. (Wang et al., 2018). Additional M2 Ser31Asn adamantane-derived inhibitors have shown similar supportive preclinical results, indicating

that these properties are fairly common for this chemical class (Hu et al., 2018). Furthermore, injection of mice with the dual-inhibitor compound **9** at up to 100 mg/kg/day resulted in no changes in body weight. Importantly, at up to 100 mg/kg/day, compound **9** also rescued mice from lethal infection of viruses containing either WT M2 or M2 Val27Ala, thereby demonstrating *in vivo* efficacy (Hu et al., 2017a). While initial results are encouraging, *in vivo* results for most adamantane derivatives remain limited and await further study.

4.2. Non-adamantane-based inhibitors

Several non-adamantane chemical scaffolds have also been successfully explored for their ability to block adamantane-resistant M2. Examples of non-adamantanes that inhibit drug-resistant M2 are shown in Table 3.

A polycyclic pyrrolidine (**17**) reported by (Rey-Carrizo et al., 2013) was reported to inhibit both WT and Val27Ala M2 by TEVC, with IC_{50} values of 3 and 0.3 μM, respectively. Another related compound (**18**) was reported by the same authors to exhibit triple inhibitory efficacy by TEVC against WT, Leu26Phe, and Val27Ala forms of M2 with IC_{50} values of 18, 8.6, and 0.7 μM, respectively (Rey-Carrizo et al., 2014). Unfortunately, the cytotoxicity of these derivatives may impede their further development as therapeutic agents. In an independent attempt to change the shape and bulk of the adamantane cage, Zhao et al. (2012) reported the discovery of pinanamine derivatives as inhibitors of M2 Ser31Asn. Specifically, an imidazole derivative of pinanamine (**19**) showed a moderate inhibitory effect against A/WSN/33 (H1N1) in a cytopathic effect inhibition assay (CPE; EC_{50} = 95.5 μM). Dong et al. (2016) subsequently reported a related compound (**20**) with improved activity against both WT A/HK/68 (H3N2) as well as A/WSN/33 (H1N1) encoding M2 Ser31Asn with EC_{50}s of 2.5 and 3.4 μM, respectively. In a separate endeavor, derivatives of spiranamine (**21**) were also explored (Balannik et al., 2009; Wang et al., 2011a). For example, a silaspirane derivative (**22**) exhibits activity against both WT and Val27Ala with 95% and 68% inhibition at 100 μM in TEVC experiments. (Wang et al., 2011b).

Another notably explored chemical class is exemplified by hexamethylene amiloride (HMA, **23**), an amiloride-based compound which is reported to block viroporins and/or replication of IAV, hepatitis C virus, HIV-1, Dengue virus, and severe acute respiratory syndrome coronavirus (SARS-CoV; Gazina and Petrou, 2012; Pervushin et al., 2009; Premkumar et al., 2004). However, HMA has several off-target effects and is cytotoxic at low micromolar concentrations (Jalily et al., 2016; Premkumar et al., 2004). Recently, a series of HMA derivatives were designed through iterative medicinal chemistry and electrophysiological testing approaches (Jalily et al., 2016). Among these compounds, **24** exhibited activity against WT M2 in single electrode voltage clamp (SEVC) experiments, which was comparable to amantadine in these studies (IC_{50} 0.2 μM vs 0.6 μM), but was not obviously toxic to cells. While **24** was found to be active against WT M2 only, an elongated derivative (**25**) exhibited dual-inhibitory effects against WT and Ser31Asn M2 in SEVC (respective IC_{50}s = 0.6 μM and 4.4 μM) and PRA (respective EC_{50}s = 40 μM and 18 μM). Additionally compound **26**, although inhibiting WT M2 with lower efficacy (20% inhibition at 100 μM) than **25** in SEVC, was more effective at inhibiting viruses encoding WT and Ser31Asn M2 in PRA (EC_{50}s = 6.9 and 1.5 μM, respectively). Preliminary data indicate that **23** exhibits stability in human microsome assays ($t_{1/2}$ = 70 min) and mouse plasma following injection *in vivo* ($t_{1/2}$ = 60 min). Moreover, injection of compound **23** at 2 mg/kg did not affect the monitored ECG or hemodynamic parameters in mice, and 200 μM of cumulative dosing of **23** over a course of 3 h did not cause obvious cardiac toxicity (P. Jalily, I. Tietjen, M. Pourrier, and D. Fedida, unpublished data).

The inhibitory effect of Cu^{2+} on M2 conductance was initially studied by Gandhi et al. (1999), where they showed that the inhibition is bi-directional across the membrane and dependent on the presence of His37. The WT protein also exhibited high specificity for Cu^{2+} and was only partially inhibited by high concentrations (1 mM) of bivalent nickel, zinc, or platinum (Gandhi et al., 1999). More recently, Gordon et al. (2017) reported the discovery of divalent copper complexes such as compound **27** as non-selective M2 inhibitors. The authors proposed that the mechanism of action of these copper complexes is independent of mutation at Leu26, Val27, or Ser31 but is instead dependent on the conduction moiety, His37, as no inhibition was observed with **27** against His37Ala mutant. Compound **27** was able to inhibit 80% of M2 proton currents at 100 μM as measured by TEVC and had an EC_{50} of 0.7 μM against A/CA/07/2009 encoding M2 Ser31Asn in PRA.

Finally, Jang et al. (2018) reported that the monovalent ionophore salinomycin (**28**) was able to counteract the proton conductance function of both influenza A and B *in vitro*. However, it indirectly inhibits M2 channel function by preventing cellular endosome acidification, similar to the mechanism of chloroquine. Salinomycin inhibited proton conduction by both M2 WT and Ser31Asn incorporated into virus-like particles (54% and 72% vs. WT and N31 at 100 μM), in addition to proton conduction by the highly divergent M2 channel of influenza B (~60%). Salinomycin also synergized with oseltamivir *in vitro*. However, while salinomycin on its own exhibited limited antiviral activity *in vivo*; it did rescue mice treated with a sub-optimal concentration of oseltamivir and lethally-infected with oseltamivir sensitive or resistant viruses. (Jang et al., 2018).

4.3. Observations from drug-resistant M2 inhibitor studies

The two-electrode voltage clamp assay remains the most effective assay for M2 ion channel studies, as it is less technically demanding and more likely to be replicated across independent laboratory groups when compared to SEVC. In general, there is a liner correlation between the percentage channel blockage from TEVC and the antiviral activity (Li et al., 2017). However, we also note that the efficacies of certain M2 inhibitors as measured by TEVC and PRA can be discordant. For example, for compounds **4**, **7**, **9**, **12**, and **15**, the IC_{50} values detected by TEVC are substantially higher than EC_{50} values by PRA. In contrast, the IC_{50} values detected for compounds **13**, **24**, and **25** by TEVC are lower than their PRA EC_{50} values. Discrepancies in both cases might arise from different binding kinetics of various M2 channel blockers (Wang et al., 2018). The IC_{50} values from TEVC or SEVC measurements are normally plotted using percentage inhibition at a given time point after compound perfusion, therefore the IC_{50} values may not accurately reflect the true binding potency of the compounds. Instead, kinetic measurements of the K_d values are a more stringent way to determine the true binding potency of M2 channel blockers. However, kinetic measurements are labor intense and are often reserved as a secondary assay to characterize lead candidates that have already shown potent antiviral activity such as compound **16**. Nevertheless, it is understandable that the lack of a straight linear correlation between the results from the *in vitro* TEVC or SEVC assay and the cellular CPE or PRA assay might also be additionally due to other factors such as a compound's membrane permeability, virus strain differences, or other off-target effects. However, this is not a specific issue related to M2 channel blockers per se, as other drug candidates commonly face this challenge as well. In some cases, discordance also extends to M2 proteins and viruses containing different mutations. For example, compound **9** inhibits M2 Val27Ala with lower IC_{50}s than M2 WT (0.3 and 18 μM, respectively), while the EC_{50}s in PRA are the opposite (i.e. 1.8 and 0.3 μM, respectively). Similar results are also seen for compounds **7**, **10**, and **20** and could reflect, for example, differences in virus strains used and/or subtle changes in the binding kinetics of these compounds against different M2 forms. Thus, as with other drug development efforts, interpretation of specific results for individual compounds must be performed carefully and on a case-by-case basis.

5. Emerging approaches for new M2 inhibitor discovery and development

The advent and improvement of electrophysiological techniques have substantially advanced our ability to directly measure the membrane currents from single cells expressing M2 or other viroporins of interest. The optimization of methods including TEVC and SEVC has also allowed us to study the fundamental biophysical properties of M2 variants and how small molecules engage and inhibit these channels. However, the inherent limitations of traditional electrophysiology such as low throughput, technical demands, and inaccessibility of the technique to many research groups have largely restricted screening and discovery of novel M2 inhibitors to a few specialized laboratories (Wang et al., 2015). Toward addressing these limitations, recently developed systems with the capacity or potential of automated electrophysiology screening could substantially reduce the time, complexity and cost associated with manual traditional patch clamp experiments, particularly in the context of SEVC. Notably, the companies Sophion (QPatch), Nanion (Patchliner) and Fluxion (IonFlux) have developed automated systems where screening of tens or hundreds of compounds could, in principle, be performed by SEVC in one day (Priest et al., 2017).

To enable high-throughput screening of M2 inhibitors with ready availability to more research groups, *S. cerevisiae* yeast strains have also been developed which are induced to express WT or adamantane-resistant M2 proteins in the presence of galactose. In these assays, M2 expression inhibits yeast growth, as measured by culture turbidity, which in turn is restored by administration of M2 inhibitors. As shown by Balgi and Roberge (2009), amantadine restored the growth of yeast expressing WT M2 from 27% of control to 95% at 1 μM. This assay was further optimized for high throughput screening: for example, the authors subsequently screened ~250,000 compounds and identified 21 new and potent inhibitors of WT M2 (Balgi et al., 2013). These reports demonstrate that growth restoration assays are a sensitive, economical and technically simple technique for high throughput screening for inhibitors of M2 and presumably other viroporins. A similar expression system using *E. coli* has also been used to assess the properties of random M2 mutations (Santner et al., 2018b), although results from these assays do not consistently agree with results obtained by TEVC (Musharrafieh et al., 2019; Santner et al., 2018a).

In a separate approach, M2 was incorporated into virus-like particles, and proton conductance was measured using a potentiometric fluorescent dye readout (Sulli et al., 2013). Using this technology, the authors successfully screened 107,572 compounds in 384-well format and discovered 19 new M2 WT-specific inhibitors with IC_{50} values ranging from 140 nM to 13 μM (Sulli et al., 2013), although no inhibitor was identified to target the drug resistant mutants of M2.

When designing drugs against viral targets, an inherent challenge is the higher degree of structural flexibility exhibited by viral proteins in comparison to many prokaryotic and eukaryotic targets (Das et al., 2010; Fischer and Hsu, 2011). Yet another challenge imposed against rational drug design is the dependence of such highly flexible proteins on their surrounding environment, which in turn affects their function. In contrast to thermostable proteins that encompass tight hydrophobic cores, viral proteins are frequently loosely packed, resulting not only in a smaller difference in energy levels between folded and unfolded states, but also a reduced contribution of random mutations or interactions with chemical inhibitors to overall stability (Paciaroni et al., 2002). This equips viruses with enormous adaptive mechanisms to buffer the deleterious effects of random mutations; even more in the case of RNA viruses which intrinsically mutate faster than DNA viruses (Tokuriki et al., 2009). These challenges also apply to M2, where until recently the lack of high-resolution structures had impeded the advancement of rational drug design. Other obstacles that have prevented the successful design of a universal M2 inhibitor include the constricted drug binding site, technical difficulties in effective measurement of

drug inhibition, and absence of reliable protocols to assess protein drug interactions.

To overcome these challenges, computation now plays a critical role in the field of rational drug design, as computers now have sufficient processing power to run virtual screening of large chemical libraries against multiple targets. While these strategies can identify multiple antiviral leads including putative viroporin inhibitors (Radosevic et al., 2019; Tietjen et al., 2015), the likelihood of false-positive hits necessitates their validation by experimental techniques. Another role of computation is now the extended ability to run complex molecular dynamics simulations in shorter times and for larger complexes to predict and visualize the interaction of viral protein domains and putative inhibitors, complexes of proteins, and simulation of complexes of viral proteins and cellular factors.

Taken together, several emerging technologies are now available to design and assess the efficacy and activity of novel M2 inhibitors. However, it is important to note that both TEVC and PRA remain "gold standards" for these studies and should be applied as secondary assays to rule out false positives obtained from higher-throughput methods.

6. Concluding remarks

The next influenza virus pandemic, albeit unpredictable, is not a matter of "if" but "when." New therapeutics, especially those that are distinct from current antivirals and with the ability to inhibit existing drug-resistant viral strains, may be essential toward mitigating the next inevitable outbreak. The M2 viroporin, a proton-dependent proton channel required for virus entry and egress, has historically been an effective antiviral target for drugs like amantadine and rimantadine. However, mutations in M2, particularly lining the pore where adamantanes interact, are now widespread and have rendered these therapies ineffective. Over the past decade, new inhibitors of drug-resistant M2 consisting of both adamantane derivatives and new chemical scaffolds have been found that inhibit M2 ion conduction, as demonstrated using both electrophysiological techniques *in vitro* influenza replication assays. The most promising leads also inhibit multiple adamantine-sensitive and resistant forms of M2 (e.g., compounds **7–10**, **12**, **17–18**, **22**, **25**), inhibit viruses with major resistance to other IAV antivirals like oseltamivir (**5**, **8**, **10**, **16**) and/or synergize with oseltamivir (**5**, **16**, **28**), exhibit high genetic barriers to resistance following long-term *in vitro* passaging (**5**, **8**, **14–16**), have supportive preclinical parameters such as good stability and low toxicity (**9**, **16**, **23**), and rescue mice from lethal infection (**9**). Going forward, further discovery of new chemical scaffolds and/or optimization of existing leads by medicinal chemistry may be enabled by emerging technologies to screen for and monitor M2 conductance. In addition, demonstration of clinical efficacy of new chemical leads remains to be achieved. The coming decade will likely show whether new M2 inhibitors can significantly add to the evolving armamentarium of antivirals to combat current and emerging seasonal and pandemic influenza strains.

List of Abbreviations

CPE	cytopathic effect inhibition assay
CC_{50}	50% cytotoxic concentration
EC_{50}	50% effective concentration
HA	hemagglutinin
HMA	hexamethylene amiloride
IAV	influenza A virus

IC$_{50}$ 50% inhibitory concentration
MDCK cells   Madin-Darby canine kidney cells
NMR   nuclear magnetic resonance
PDB   Protein Data Bank
PRA   plaque reduction assay
SARS-CoV   severe acute respiratory syndrome coronavirus
SEVC   single electrode voltage clamp
TEVC   two electrode voltage clamp
WT   wild-type

References

Acharya, R., Carnevale, V., Fiorin, G., Levine, B.G., Polishchuk, A.L., Balannik, V., Samish, I., Lamb, R.A., Pinto, L.H., DeGrado, W.F., Klein, M.L., 2010. Structure and mechanism of proton transport through the transmembrane tetrameric M2 protein bundle of the influenza A virus. Proc. Natl. Acad. Sci. Unit. States Am. 107, 15075–15080. https://doi.org/10.1073/pnas.1007071107.

Aldabe, R., Barco, A., Carrasco, L., 1996. Membrane permeabilization by poliovirus proteins 2B and 2BC. J. Biol. Chem. 271, 23134–23137. https://doi.org/10.1074/JBC.271.38.23134.

Aldrich, P.E., Hermann, E.C., Meier, W.E., Paulshock, M., Prichard, W.W., Synder, J.A., Watts, J.C., 1971. Antiviral agents. 2. Structure-activity relations of compounds related to 1-adamantanamine. J. Med. Chem. 14, 535–543. https://doi.org/10.1021/jm00288a019.

Alvarado-Facundo, E., Gao, Y., Ribas-Aparicio, R.M., Jiménez-Alberto, A., Weiss, C.D., Wang, W., 2015. Influenza virus M2 protein ion channel activity helps to maintain pandemic 2009 H1N1 virus hemagglutinin fusion competence during transport to the cell surface. J. Virol. 89, 1975–1985. https://doi.org/10.1128/JVI.03253-14.

Balannik, V., Carnevale, V., Fiorin, G., Levine, B.G., Lamb, R.a., Klein, M.L., DeGrado, W.F., Pinto, L.H., 2010. Functional studies and modeling of pore-lining residue mutants of the influenza A virus M2 ion channel. Biochemistry 49, 696–708. https://doi.org/10.1021/bi901799k.

Balannik, V., Wang, J., Ohigashi, Y., Jing, X., Magavern, E., Lamb, R.A., DeGrado, W.F., Pinto, L.H., 2009. Design and pharmacological characterization of inhibitors of amantadine-resistant mutants of the M2 ion channel of influenza A virus. Biochemistry 48, 11872–11882. https://doi.org/10.1021/bi9014488.

Balgi, A.D., Roberge, M., 2009. Screening for Chemical Inhibitors of Heterologous Proteins Expressed in Yeast Using a Simple Growth-Restoration Assay. Humana Press, Totowa, NJ, pp. 125–137. https://doi.org/10.1007/978-1-60327-545-3_9.

Balgi, A.D., Wang, J., Cheng, D.Y.H., Ma, C., Pfeifer, T.A., Shimizu, Y., Anderson, H.J., Pinto, L.H., Lamb, R.A., DeGrado, W.F., Roberge, M., 2013. Inhibitors of the influenza A virus M2 proton channel discovered using a high-throughput yeast growth restoration assay. PLoS One 8, e55271. https://doi.org/10.1371/journal.pone.0055271.

Barniol-Xicota, M., Gazzarrini, S., Torres, E., Hu, Y., Wang, J., Naesens, L., Moroni, A., Vázquez, S., 2017. Slow but steady wins the race: dissimilarities among new dual inhibitors of the wild-type and the V27A mutant M2 channels of influenza A virus. J. Med. Chem. 60, 3727–3738. https://doi.org/10.1021/acs.jmedchem.6b01758.

Bodelón, G., Labrada, L., Martínez-Costas, J., Benavente, J., 2002. Modification of late membrane permeability in avian reovirus-infected cells: viroporin activity of the S1-encoded nonstructural p10 protein. J. Biol. Chem. 277, 17789–17796. https://doi.org/10.1074/jbc.M202018200.

Bright, R.A., Medina, M.J., Xu, X., Perez-Oronoz, G., Wallis, T.R., Davis, X.M., Povinelli, L., Cox, N.J., Klimov, A.I., 2005. Incidence of adamantane resistance among influenza A (H3N2) viruses isolated worldwide from 1994 to 2005: a cause for concern. Lancet 366, 1175–1181. https://doi.org/10.1016/S0140-6736(05)67338-2.

Bright, R.A., Shay, D.K., Shu, B., Cox, N.J., Klimov, A.I., 2006. Adamantane resistance among influenza A viruses isolated early during the 2005-2006 influenza season in the United States. J. Am. Med. Assoc. 295, 891. https://doi.org/10.1001/jama.295.8.joc60020.

Bui, M., Whittaker, G., Helenius, A., 1996. Effect of M1 protein and low pH on nuclear transport of influenza virus ribonucleoproteins. J. Virol. 70, 8391–8401.

Cady, S., Wang, T., Hong, M., 2011a. Membrane-dependent effects of a cytoplasmic helix on the structure and drug binding of the influenza virus M2 protein. J. Am. Chem. Soc. 133, 11572–11579. https://doi.org/10.1021/ja202051n.

Cady, S.D., Luo, W., Hu, F., Hong, M., 2009a. Structure and function of the influenza A M2 proton channel. Biochemistry 48, 7356–7364. https://doi.org/10.1021/bi9008837.

Cady, S.D., Mishanina, T.V., Hong, M., 2009b. Structure of amantadine-bound M2 transmembrane peptide of influenza A in lipid bilayers from magic-angle-spinning solid-state NMR: the role of Ser31 in amantadine binding. J. Mol. Biol. 385, 1127–1141. https://doi.org/10.1016/j.jmb.2008.11.022.

Cady, S.D., Schmidt-Rohr, K., Wang, J., Soto, C.S., Degrado, W.F., Hong, M., 2010. Structure of the amantadine binding site of influenza M2 proton channels in lipid bilayers. Nature 463, 689–692. https://doi.org/10.1038/nature08722.

Cady, S.D., Wang, J., Wu, Y., Degrado, W.F., Hong, M., 2011b. Specific binding of adamantane drugs and direction of their polar amines in the pore of the influenza M2 transmembrane domain in lipid bilayers and dodecylphosphocholine micelles determined by NMR spectroscopy. J. Am. Chem. Soc. 133, 4274–4284. https://doi.org/10.1021/ja102581n.

Carpenter, E.P., Beis, K., Cameron, A.D., Iwata, S., 2008. Overcoming the challenges of membrane protein crystallography. Curr. Opin. Struct. Biol. 18, 581–586. https://doi.

org/10.1016/j.sbi.2008.07.001.

Castaño-Rodriguez, C., Honrubia, J.M., Gutiérrez-Álvarez, J., DeDiego, M.L., Nieto-Torres, J.L., Jimenez-Guardeño, J.M., Regla-Nava, J.A., Fernandez-Delgado, R., Verdia-Báguena, C., Queralt-Martín, M., Kochan, G., Perlman, S., Aguilella, V.M., Sola, I., Enjuanes, L., 2018. Role of severe acute respiratory syndrome coronavirus viroporins E, 3a, and 8a in replication and pathogenesis. MBio 9 https://doi.org/10.1128/mBio.02325-17. e02325-17.

CDC, 2018. Estimated Influenza Illnesses, Medical Visits, Hospitalizations, and Deaths in the United States — 2017–2018 Influenza Season. CDC [WWW Document]. Influ. URL. https://www.cdc.gov/flu/about/burden/2017-2018.htm accessed 7.20.19.

Chen, B.J., Leser, G.P., Jackson, D., Lamb, R.A., 2008. The influenza virus M2 protein cytoplasmic tail interacts with the M1 protein and influences virus assembly at the site of virus budding. J. Virol. 82, 10059–10070. https://doi.org/10.1128/JVI.01184-08.

Chizhmakov, I.V., Geraghty, F.M., Ogden, D.C., Hayhurst, A., Antoniou, M., Hay, a J., 1996. Selective proton permeability and pH regulation of the influenza virus M2 channel expressed in mouse erythroleukaemia cells. J. Physiol. 494 (Pt 2), 329–336.

Chuang, G.Y., Kozakov, D., Brenke, R., Beglov, D., Guarnieri, F., Vajda, S., 2009. Binding hot spots and amantadine orientation in the influenza A virus M2 proton channel. Biophys. J. 97, 2846–2853. https://doi.org/10.1016/j.bpj.2009.09.004.

Ciampor, F., Bayley, P.M., Nermut, M.V., Hirst, E.M., Sugrue, R.J., Hay, A.J., 1992. Evidence that the amantadine-induced, M2-mediated conversion of influenza A virus hemagglutinin to the low pH conformation occurs in an acidic trans Golgi compartment. Virology 188, 14–24.

Cross, T.A., Dong, H., Sharma, M., Busath, D.D., Zhou, H.-X., 2012. M2 protein from Influenza A: from multiple structures to biophysical and functional insights. Curr. Opin. Virol. 2, 128–133. https://doi.org/10.1016/j.coviro.2012.01.005.

Das, K., Aramini, J.M., Ma, L.-C., Krug, R.M., Arnold, E., 2010. Structures of influenza A proteins and insights into antiviral drug targets. Nat. Struct. Mol. Biol. 17, 530–538. https://doi.org/10.1038/nsmb.1779.

Davies, W.L., Grunert, R.R., Haff, R.F., McGahen, J.W., Neumayer, E.M., Paulshock, M., Watts, J.C., Wood, T.R., Hermann, E.C., Hoffmann, C.E., 1964. Antiviral activity of 1-adamantanamine (amantadine). Science (80) 144, 862–863. https://doi.org/10.1126/science.144.3620.862.

Deyde, V.M., Xu, X., Bright, R.A., Shaw, M., Smith, C.B., Zhang, Y., Shu, Y., Gubareva, L.V., Cox, N.J., Klimov, A.I., 2007. Surveillance of resistance to adamantanes among influenza A(H3N2) and A(H1N1) viruses isolated worldwide. J. Infect. Dis. 196, 249–257. https://doi.org/10.1086/518936.

Dong, G., Peng, C., Luo, J., Wang, C., Han, L., Wu, B., Ji, G., He, H., 2015. Adamantane-resistant influenza A viruses in the world (1902–2013): frequency and distribution of M2 gene mutations. PLoS One 10, e0119115. https://doi.org/10.1371/journal.pone.0119115.

Dong, J., Chen, S., Li, R., Cui, W., Jiang, H., Ling, Y., Yang, Z., Hu, W., 2016. Imidazole-based pinanamine derivatives: discovery of dual inhibitors of the wild-type and drug-resistant mutant of the influenza A virus. https://doi.org/10.1016/j.ejmech.2015.12.013.

Drakopoulos, A., Tzitzoglaki, C., Ma, C., Freudenberger, K., Hoffmann, A., Hu, Y., Gauglitz, G., Schmidtke, M., Wang, J., Kolocouris, A., 2017. Affinity of rimantadine enantiomers against influenza A/M2 protein revisited. ACS Med. Chem. Lett. 8, 145–150. https://doi.org/10.1021/acsmedchemlett.6b00311.

Du, J., Cross, T.A., Zhou, H.X., 2012. Recent progress in structure-based anti-influenza drug design. Drug Discov. Today 17, 1111–1120. https://doi.org/10.1016/j.drudis.2012.06.002.

Duff, K.C., Ashley, R.H., 1992. The transmembrane domain of influenza A M2 protein forms amantadine-sensitive proton channels in planar lipid bilayers. Virology 190, 485–489.

Duque, M.D., Ma, C., Torres, E., Wang, J., Naesens, L., Juárez-Jiménez, J., Camps, P., Luque, F.J., Degrado, W.F., Lamb, R.A., Pinto, L.H., Vázquez, S., 2011. Exploring the size limit of templates for inhibitors of the M2 ion channel of influenza A virus. J. Med. Chem. 54, 2646–2657. https://doi.org/10.1021/jm101334y.

Durrant, M.G., Eggett, D.L., Busath, D.D., 2014. Investigation of a Recent Rise of Dual Amantadine-Resistance Mutations in the Influenza A M2 Sequence. https://doi.org/10.1186/1471-2156-16-S2-S3.

Fiore, A.E., Fry, A., Shay, D., Gubareva, L., Bresee, J.S., Uyeki, T.M., Centers for Disease Control and Prevention (CDC), 2011. Antiviral agents for the treatment and chemoprophylaxis of influenza — recommendations of the Advisory Committee on Immunization Practices (ACIP). MMWR Recomm. Rep. (Morb. Mortal. Wkly. Rep.) 60, 1–24.

Fischer, W.B., Hsu, H.J., 2011. Viral channel forming proteins - modeling the target. Biochim. Biophys. Acta Biomembr. 1808, 561–571. https://doi.org/10.1016/j.bbamem.2010.05.014.

Furuse, Y., Suzuki, A., Kamigaki, T., Oshitani, H., 2009a. Evolution of the M gene of the influenza A virus in different host species: large-scale sequence analysis. Virol. J. 6, 67. https://doi.org/10.1186/1743-422X-6-67.

Furuse, Y., Suzuki, A., Oshitani, H., 2009b. Large-scale sequence analysis of M gene of influenza A viruses from different species: mechanisms for emergence and spread of amantadine resistance. Antimicrob. Agents Chemother. 53, 4457–4463. https://doi.org/10.1128/AAC.00650-09.

Gan, S.-W., Tan, E., Lin, X., Yu, D., Wang, J., Tan, G.M.-Y., Vararattanavech, A., Yeo, C.Y., Soon, C.H., Soong, T.W., Pervushin, K., Torres, J., 2012. The small hydrophobic protein of the human respiratory syncytial virus forms pentameric ion channels. J. Biol. Chem. 287, 24671–24689. https://doi.org/10.1074/jbc.M111.332791.

Gandhi, C.S., Shuck, K., Lear, J.D., Dieckmann, G.R., DeGrado, W.F., Lamb, R.A., Pinto, L.H., 1999. Cu(II) inhibition of the proton translocation machinery of the influenza a virus M2 protein. J. Biol. Chem. 274, 5474–5482. https://doi.org/10.1074/jbc.274.9.5474.

Gazina, E.V., Petrou, S., 2012. Viral targets of acylguanidines. Drug Discov. Today 17, 1039–1043. https://doi.org/10.1016/j.drudis.2012.05.002.

Gleed, M.L., Ioannidis, H., Kolocouris, A., Busath, D.D., 2015. Resistance-Mutation (N31) Effects on Drug Orientation and Channel Hydration in Amantadine-Bound Influenza A M2. https://doi.org/10.1021/acs.jpcb.5b05808.

Gordon, N.A., McGuire, K.L., Wallentine, S.K., Mohl, G.A., Lynch, J.D., Harrison, R.G., Busath, D.D., 2017. Divalent copper complexes as influenza A M2 inhibitors. Antivir. Res. 147, 100–106. https://doi.org/10.1016/j.antiviral.2017.10.009.

Grambas, S., Bennett, M.S., Hay, A.J., 1992. Influence of amantadine resistance mutations on the pH regulatory function of the M2 protein of influenza A viruses. Virology 191, 541–549. https://doi.org/10.1016/0042-6822(92)90229-I.

Gu, R.-X., Liu, L.A., Wei, D.-Q., 2013. Structural and energetic analysis of drug inhibition of the influenza A M2 proton channel. Trends Pharmacol. Sci. 34, 571–580. https://doi.org/10.1016/j.tips.2013.08.003.

Gu, R.X., Liu, L.A., Wei, D.Q., Du, J.G., Liu, L., Liu, H., 2011. Free energy calculations on the two drug binding sites in the M2 proton channel. J. Am. Chem. Soc. 133, 10817–10825. https://doi.org/10.1021/ja1114198.

Gutman, O., Danieli, T., White, J.M., Henis, Y.I., 1993. Effects of exposure to low pH on the lateral mobility of influenza hemagglutinin expressed at the cell surface: correlation between mobility inhibition and inactivation. Biochemistry 32, 101–106. https://doi.org/10.1021/bi00052a014.

Hayden, F.G., De Jong, M.D., 2011. Emerging influenza antiviral resistance threats. J. Infect. Dis. https://doi.org/10.1093/infdis/jiq012.

Holsinger, L.J., Nichani, D., Pinto, L.H., Lamb, R. a, 1994. Influenza A virus M2 ion channel protein: a structure-function analysis. J. Virol. 68, 1551–1563.

Holsinger, L.J., Shaughnessy, M.A., Micko, A., Pinto, L.H., Lamb, R.A., 1995. Analysis of the posttranslational modifications of the influenza virus M2 protein. J. Virol. 69, 1219–1225.

Hong, M., DeGrado, W.F., 2012. Structural basis for proton conduction and inhibition by the influenza M2 protein. Protein Sci. 21, 1620–1633. https://doi.org/10.1002/pro.2158.

Hu, F., Luo, W., Hong, M., 2010. Mechanisms of proton conduction and gating in influenza M2 proton channels from solid-state NMR. Science (80) 330, 505–508. https://doi.org/10.1126/science.1191714.

Hu, Y., Hau, R.K., Wang, Y., Tuohy, P., Zhang, Y., Xu, S., Ma, C., Wang, J., 2018. Structure-Property relationship studies of influenza A virus AM2-S31N proton channel blockers. ACS Med. Chem. Lett. 9, 1111–1116. https://doi.org/10.1021/acsmedchemlett.8b00336.

Hu, Y., Musharrafieh, R., Ma, C., Zhang, J., Smee, D.F., DeGrado, W.F., Wang, J., 2017a. An M2-V27A channel blocker demonstrates potent in vitro and in vivo antiviral activities against amantadine-sensitive and -resistant influenza A viruses. Antivir. Res. 140, 45–54. https://doi.org/10.1016/j.antiviral.2017.01.006.

Hu, Y., Wang, Y., Li, F., Ma, C., Wang, J., 2017b. Design and expeditious synthesis of organosilanes as potent antivirals targeting multidrug-resistant influenza A viruses. Eur. J. Med. Chem. 135, 70–76. https://doi.org/10.1016/j.ejmech.2017.04.038.

Hurt, A.C., 2014. The epidemiology and spread of drug resistant human influenza viruses. Curr. Opin. Virol. 8, 22–29. https://doi.org/10.1016/j.coviro.2014.04.009.

Jalily, P.H., Eldstrom, J., Miller, S.C., Kwan, D.C., Tai, S.S.-H., Chou, D., Niikura, M., Tietjen, I., Fedida, D., 2016. Mechanisms of action of novel influenza A/M2 viroporin inhibitors derived from hexamethylene amiloride. Mol. Pharmacol. 90, 80–95. https://doi.org/10.1124/mol.115.102731.

Jang, Y., Soo Shin, J., Yoon, Y.-S., Young Go, Y., Won Lee, H., Seung Kwon, O., Park, S., Park, M.-S., Kim, M., Jae Jung, E.U., 2018. Salinomycin inhibits influenza virus infection by disrupting endosomal acidification and viral matrix protein 2 function salinomycin inhibits influenza virus infection by disrupting endosomal acidification and viral matrix protein 2 function VACCINES AND. jvi.asm.org 1 J. Virol. 92, 1441–1459. https://doi.org/10.1128/JVI.01441-18.

Jing, X., Ma, C., Ohigashi, Y., Oliveira, F.A., Jardetzky, T.S., Pinto, L.H., Lamb, R.A., 2008. Functional studies indicate amantadine binds to the pore of the influenza A virus M2 proton-selective ion channel. Proc. Natl. Acad. Sci. Unit. States Am. 105, 10967–10972. https://doi.org/10.1073/pnas.0804958105.

Joubert, D.A., Blasdell, K.R., Audsley, M.D., Trinidad, L., Monaghan, P., Dave, K.A., Lieu, K.G., Amos-Ritchie, R., Jans, D.A., Moseley, G.W., Gorman, J.J., Walker, P.J., 2014. Bovine Ephemeral Fever Rhabdovirus α1 Protein Has Viroporin-like Properties and Binds Importin β1 and Importin 7. https://doi.org/10.1128/JVI.01812-13.

Kabsch, K., Alonso, A., 2002. The human papillomavirus type 16 E5 protein impairs TRAIL- and FasL-mediated apoptosis in HaCaT cells by different mechanisms. J. Virol. 76, 12162–12172. https://doi.org/10.1128/JVI.76.23.12162-12172.2002.

Kesinger, E., Liu, J., Jensen, A., Chia, C.P., Demers, A., Moriyama, H., 2018. Influenza D virus M2 protein exhibits ion channel activity in Xenopus laevis oocytes. PLoS One 13, e0199227. https://doi.org/10.1371/journal.pone.0199227.

Keyser, L.A., Karl, M., Nafziger, A.N., Bertino, J.S., 2000. Comparison of central nervous system Adverse effects of amantadine and rimantadine used as sequential prophylaxis of influenza A in elderly nursing home patients. Arch. Intern. Med. 160, 1485. https://doi.org/10.1001/archinte.160.10.1485.

Khurana, E., Devane, R.H., Dal Peraro, M., Klein, M.L., 2011. Computational study of drug binding to the membrane-bound tetrameric M2 peptide bundle from influenza A virus. Biochim. Biophys. Acta 1808, 530–537. https://doi.org/10.1016/j.bbamem.2010.03.025.

Kolokouris, D., Kalenderoglou, I., Lagarias, P., Kolocouris, A., 2019. Spotting differences in molecular dynamic simulations of influenza A M2 protein-ligand complexes by varying M2 construct, lipid bilayer and force field. ChemRxiv. https://doi.org/10.26434/chemrxiv.11365943.v1.

Kovacs, F.A., Denny, J.K., Song, Z., Quine, J.R., Cross, T.A., 2000. Helix tilt of the M2 transmembrane peptide from influenza A virus: an intrinsic property. J. Mol. Biol. 295, 117–125. https://doi.org/10.1006/jmbi.1999.3322.

Lamb, R.A., Krug, R.M., 2001. Orthomyxoviridae: the Viruses and Their Replication, fourth ed. Lippincott Williams & Wilkins, Philadelphia.

Lamb, R.A., Choppin, P.W., 1981. Identification of a second protein (M2) encoded by RNA segment 7 of influenza virus. Virology 112, 729–737. https://doi.org/10.1016/0042-6822(81)90317-2.

Lamb, R.A., Lai, C.J., 1981. Conservation of the influenza virus membrane protein (M1) amino acid sequence and an open reading frame of RNA segment 7 encoding a second protein (M2) in H1N1 and H3N2 strains. Virology 112, 746–751. https://doi.org/10.1016/0042-6822(81)90319-6.

Lamb, R.A., Lai, C.J., Choppin, P.W., 1981. Sequences of mRNAs derived from genome RNA segment 7 of influenza virus: colinear and interrupted mRNAs code for overlapping proteins. Proc. Natl. Acad. Sci. Unit. States Am. 78, 4170–4174. https://doi.org/10.1073/pnas.78.7.4170.

Lamb, R.A., Zebedee, S.L., Richardson, C.D., 1985. Influenza virus M2 protein is an integral membrane protein expressed on the infected-cell surface. Cell 40, 627–633. https://doi.org/10.1016/0092-8674(85)90211-9.

Leiding, T., Wang, J., Martinsson, J., DeGrado, W.F., Arskold, S.P., 2010. Proton and cation transport activity of the M2 proton channel from influenza A virus. Proc. Natl. Acad. Sci. Unit. States Am. 107, 15409–15414. https://doi.org/10.1073/pnas.1009997107.

Li, F., Hu, Y., Wang, Y., Ma, C., Wang, J., 2017. Expeditious Lead Optimization of Isoxazole-Containing Influenza A Virus M2-S31n Inhibitors Using the Suzuki−Miyaura Cross-Coupling Reaction. https://doi.org/10.1021/acs.jmedchem.6b01852.

Li, F., Ma, C., Degrado, W.F., Wang, J., 2016a. Discovery of highly potent inhibitors targeting the predominant drug-resistant S31N mutant of the influenza A virus M2 proton channel. J. Med. Chem. 59, 1207–1216. https://doi.org/10.1021/acs.jmedchem.5b01910.

Li, F., Ma, C., Hu, Y., Wang, Y., Wang, J., 2016b. Discovery of potent antivirals against amantadine-resistant influenza A viruses by targeting the M2-S31N proton channel Graphical abstract Keywords Influenza A virus; M2 proton channel. M2-S31N inhibitor HHS Public Access 2, 726–733. https://doi.org/10.1021/acsinfecdis.6b00130.

Li, S., Sieben, C., Ludwig, K., Hö, C.T., Chiantia, S., Herrmann, A., Eghiaian, F., Schaap, I.A.T., 2014. pH-Controlled Two-step Uncoating of Influenza Virus. https://doi.org/10.1016/j.bpj.2014.02.018.

Ma, C., Fiorin, G., Carnevale, V., Wang, J., Lamb, R.A., Klein, M.L., Wu, Y., Pinto, L.H., DeGradi, W.F., 2013. Asp44 stabilizes the Trp41 gate of the M2 proteon channel of influenza A virus. Structure 21, 2033–2041. https://doi.org/10.1016/j.str.2013.08.029.

Ma, C., Polishchuk, A.L., Ohigashi, Y., Stouffer, A.L., Schon, A., Magavern, E., Jing, X., Lear, J.D., Freire, E., Lamb, R.A., DeGrado, W.F., Pinto, L.H., 2009. Identification of the functional core of the influenza A virus A/M2 proton-selective ion channel. Proc. Natl. Acad. Sci. Unit. States Am. 106, 12283–12288. https://doi.org/10.1073/pnas.0905726106.

Ma, C., Zhang, J., Wang, J., 2016. Pharmacological characterization of the spectrum of antiviral activity and genetic barrier to drug resistance of M2-S31N channel blockers. Mol. Pharmacol. 90, 188–198. https://doi.org/10.1124/mol.116.105346.

Madan, V., Bartenschlager, R., Carrasco, L., Nieva, J.L., 2015. Structural and functional properties of the hepatitis C virus p7 viroporin. Viruses 7, 4461–4481. https://doi.org/10.3390/v7082826.

Martin, K., Heleniust, A., 1991. Nuclear transport of influenza virus ribonucleoproteins: the viral matrix protein (ml) promotes export and inhibits import. Cell.

Mould, J.a., Paterson, R.G., Takeda, M., Ohigashi, Y., Venkataraman, P., Lamb, R.a., Pinto, L.H., 2003. Influenza B virus BM2 protein has ion channel activity that conducts protons across membranes. Dev. Cell 5, 175–184. https://doi.org/10.1016/S1534-5807(03)00190-4.

Musharrafieh, R., Lagarias, P.I., Ma, C., Tan, G.S., Kolocouris, A., Wang, J., 2019. The L46P mutant confers a novel allosteric mechanism of resistance toward the influenza A virus M2 S31N proton channel blockers. Mol. Pharmacol. 96, 148–157. https://doi.org/10.1124/mol.119.116640.

Musharrafieh, R., Ma, C., Wang, J., 2018. Profiling the in vitro drug-resistance mechanism of influenza A viruses towards the AM2-S31N proton channel blockers. Antivir. Res. 153, 10–22. https://doi.org/10.1016/j.antiviral.2018.03.002.

Nelson, M.I., Simonsen, L., Viboud, C., Miller, M.A., Holmes, E.C., 2009. The origin and global emergence of adamantane resistant A/H3N2 influenza viruses. Virology 388, 270–278. https://doi.org/10.1016/j.virol.2009.03.026.

Nieto-Torres, J., Verdiá-Báguena, C., Castaño-Rodriguez, C., Aguilella, V., Enjuanes, L., 2015. Relevance of viroporin ion channel activity on viral replication and pathogenesis. Viruses 7, 3552–3573. https://doi.org/10.3390/v7072786.

Nieva, J.L., Madan, V., Carrasco, L., 2012. Viroporins: Structure and biological functions. Nat. Rev. Microbiol. 10, 563–574. https://doi.org/10.1038/nrmicro2820.

Ouyang, B., Chou, J.J., 2014. The minimalist architectures of viroporins and their therapeutic implications. Biochim. Biophys. Acta Biomembr. 1838, 1058–1067. https://doi.org/10.1016/j.bbamem.2013.09.004.

Paciaroni, A., Cinelli, S., Onori, G., 2002. Effect of the environment on the protein dynamical transition: a neutron scattering study. Biophys. J. 83, 1157–1164. https://doi.org/10.1016/S0006-3495(02)75239-9.

Pekosz, A., Lamb, R.A., 1998. Influenza C virus CM2 integral membrane glycoprotein is produced from a polypeptide precursor by cleavage of an internal signal sequence. Microbiology 95, 13233–13238.

Pervushin, K., Tan, E., Parthasarathy, K., Lin, X., Jiang, F.L., Yu, D., Vararattanavech, A., Soong, T.W., Liu, D.X., Torres, J., 2009. Structure and inhibition of the SARS coronavirus envelope protein ion channel. PLoS Pathog. 5, e1000511. https://doi.org/10.1371/journal.ppat.1000511.

Pielak, R.M., Chou, J.J., 2010. Solution NMR structure of the V27A drug resistant mutant

of influenza A M2 channel. Biochem. Biophys. Res. Commun. 401, 58–63. https://doi.org/10.1016/j.bbrc.2010.09.008.

Pielak, R.M., Oxenoid, K., Chou, J.J., 2011. Structural investigation of rimantadine inhibition of the AM2-BM2 chimera channel of influenza viruses. Structure 19, 1655–1663. https://doi.org/10.1016/j.str.2011.09.003.

Pielak, R.M., Schnell, J.R., Chou, J.J., 2009. Mechanism of drug inhibition and drug resistance of influenza A M2 channel. Proc. Natl. Acad. Sci. Unit. States Am. 106, 7379–7384. https://doi.org/10.1073/pnas.0902548106.

Pinto, L.H., Holsinger, L.J., Lamb, R. a, 1992. Influenza virus M2 protein has ion channel activity. Cell 69, 517–528. https://doi.org/10.1016/0092-8674(92)90452-I.

Pinto, L.H., Lamb, R. a, 2006. The M2 proton channels of influenza A and B viruses. J. Biol. Chem. 281, 8997–9000. https://doi.org/10.1074/jbc.R500020200.

Premkumar, A., Wilson, L., Ewart, G., Gage, P., 2004. Cation-selective ion channels formed by p7 of hepatitis C virus are blocked by hexamethylene amiloride. FEBS Lett. 557, 99–103. https://doi.org/10.1016/S0014-5793(03)01453-4.

Priest, B.T., Cerne, R., Krambis, M.J., Schmalhofer, W.A., Wakulchik, M., Wilenkin, B., Burris, K.D., 2017. Automated Electrophysiology Assays, Assay Guidance Manual. Eli Lilly & Company and the National Center for Advancing Translational Sciences.

Radosevic, D., Sencanski, M., Perovic, V., Veljkovic, N., Prljic, J., Veljkovic, V., Mantlo, E., Bukreyeva, N., Paessler, S., Glisic, S., 2019. Virtual screen for repurposing of drugs for candidate influenza A M2 ion-channel inhibitors. Front. Cell. Infect. Microbiol. 9, 67. https://doi.org/10.3389/fcimb.2019.00067.

Renaud, C., Kuypers, J., Englund, J.A., 2011. Emerging oseltamivir resistance in seasonal and pandemic influenza A/H1N1. J. Clin. Virol. 52, 70–78. https://doi.org/10.1016/j.jcv.2011.05.019.

Rey-Carrizo, M., Barniol-Xicota, M., Ma, C., Frigolé-Vivas, M., Torres, E., Naesens, L., Llabrés, S., Juárez-Jiménez, J., Luque, F.J., DeGrado, W.F., Lamb, R.A., Pinto, L.H., Vázquez, S., 2014. Easily accessible polycyclic amines that inhibit the wild-type and amantadine-resistant mutants of the M2 channel of influenza A virus. J. Med. Chem. 57, 5738–5747. https://doi.org/10.1021/jm5005804.

Rey-Carrizo, M., Torres, E., Ma, C., Barniol-Xicota, M., Wang, J., Wu, Y., Naesens, L., Degrado, W.F., Lamb, R.A., Pinto, L.H., Vázquez, S., 2013. 3-azatetracyclo [5.2.1.15,8.01,5]undecane Derivatives: from wild-type inhibitors of the M2 ion channel of influenza A virus to derivatives with potent activity against the V27A mutant. J. Med. Chem. 56, 9265–9274. https://doi.org/10.1021/jm401340p.

Rolfes, M.A., Flannery, B., Chung, J., O'Halloran, A., Garg, S., Belongia, E.A., Gaglani, M., Zimmerman, R., Jackson, M.L., Monto, A.S., Alden, N.B., Anderson, E., Bennett, N.M., Billing, L., Eckel, S., Kirley, P.D., Lynfield, R., Monroe, M.L., Spencer, M., Spina, N., Talbot, H.K., Thomas, A., Torres, S., Yousey-Hindes, K., Singleton, J., Patel, M., Reed, C., Fry, A.M., 2019. Effects of influenza vaccination in the United States during the 2017–2018 influenza season. Clin. Infect. Dis. https://doi.org/10.1093/cid/ciz075.

Rosenberg, M.R., Casarotto, M.G., 2010. Coexistence of two adamantane binding sites in the influenza A M2 ion channel. Proc. Natl. Acad. Sci. Unit. States Am. 107, 13866–13871. https://doi.org/10.1073/pnas.1002051107.

Rossman, J., Lamb, R., 2011. Influenza virus assembly and budding. Virology 411, 229–236. https://doi.org/10.1016/j.virol.2010.12.003.Influenza.

Rossman, J.S., Jing, X., Leser, G.P., Lamb, R.A., 2010. Influenza virus M2 protein mediates ESCRT-independent membrane scission. Cell 142, 902–913. https://doi.org/10.1016/j.cell.2010.08.029.

Santner, P., da Silva Martins, M., Kampmeyer, C., Hartmann-Petersen, R., Laursen, J.S., Stein, A., Olsen, C.A., Arkin, I.T., Winther, J.R., Willemoe, M., Lindorff-Larsen, K., 2018a. Random mutagenesis analysis of the influenza A M2 proton channel reveals novel resistance mutants. Cite This Biochem 57, 5968. https://doi.org/10.1021/acs.biochem.8b00722.

Santner, P., Martins, J.M. da S., Laursen, J.S., Behrendt, L., Riber, L., Olsen, C.A., Arkin, I.T., Winther, J.R., Willemoës, M., Lindorff-Larsen, K., 2018b. A robust proton flux (pHlux) assay for studying the function and inhibition of the influenza A M2 proton channel. Biochemistry 57, 5949–5956. https://doi.org/10.1021/acs.biochem.8b00721.

Schnell, J.R., Chou, J.J., 2008. Structure and mechanism of the M2 proton channel of influenza A virus. Nature 451, 591–595. https://doi.org/10.1038/nature06531.

Scholtissek, C., Quack, G., Klenk, H.D., Webster, R.G., 1998. How to overcome resistance of influenza A viruses against adamantane derivatives. Antivir. Res. 37, 83–95. https://doi.org/10.1016/S0166-3542(97)00061-2.

Schwab, R.S., England, A.C., Poskanzer, D.C., Young, R.R., 1969. Amantadine in the treatment of Parkinson's disease. J. Am. Med. Assoc. 208, 1168–1170.

Sharma, M., Yi, M., Dong, H., Qin, H., Peterson, E., Busath, D.D., Zhou, H.-X., Cross, T.A., 2010. Insight into the mechanism of the influenza A proton channel from a structure in a lipid bilayer. Science (80-) 330, 509–512. https://doi.org/10.1126/science.1191750.

Shimbo, K., Brassard, D.L., Lamb, R.A., Pinto, L.H., 1996. Ion selectivity and activation of the M2ion channel of influenza virus. Biophys. J. 70, 1335–1346. https://doi.org/10.1016/S0006-3495(96)79690-X.

Stauffer, S., Feng, Y., Nebioglu, F., Heilig, R., Picotti, P., Helenius, A., 2014. Stepwise priming by acidic pH and a high K concentration is required for efficient uncoating of influenza A virus cores after penetration. J. Virol. 88, 13029–13046. https://doi.org/10.1128/JVI.01430-14.

Stouffer, A.L., Acharya, R., Salom, D., Levine, A.S., Di Costanzo, L., Soto, C.S., Tereshko, V., Nanda, V., Stayrook, S., DeGrado, W.F., 2008. Structural basis for the function and inhibition of an influenza virus proton channel. Nature 451, 596–599. https://doi.org/10.1038/nature06528.

Strebel, K., 2014. HIV-1 Vpu - an ion channel in search of a job. Biochim. Biophys. Acta 1838, 1074–1081. https://doi.org/10.1016/j.bbamem.2013.06.029.

Sugrue, R.J., Bahadur, G., Zambon, M.C., Hall-Smith, M., Douglas, A., Hay, a J., 1990. Specific structural alteration of the influenza haemagglutinin by amantadine. EMBO J. 9, 3469–3476.

Sulli, C., Banik, S.S.R., Schilling, J., Moser, A., Xiang, X., Payne, R., Wanless, A., Willis, S.H., Paes, C., Rucker, J.B., Doranz, B.J., 2013. Detection of proton movement directly across viral membranes to identify novel influenza virus M2 inhibitors. J. Virol. 87, 10679–10686. https://doi.org/10.1128/JVI.01190-13.

Suzuki, T., Orba, Y., Okada, Y., Sunden, Y., Kimura, T., Tanaka, S., Nagashima, K., Hall, W.W., Sawa, H., 2010. The human polyoma JC virus agnoprotein acts as a viroporin. PLoS Pathog. 6. https://doi.org/10.1371/journal.ppat.1000801.

Takeda, M., Leser, G.P., Russell, C.J., Lamb, R.A., 2003. Influenza virus hemagglutinin concentrates in lipid raft microdomains for efficient viral fusion. Proc. Natl. Acad. Sci. U.S.A. 100, 14610–14617. https://doi.org/10.1073/pnas.2235620100.

Tang, Y., Zaitseva, F., Lamb, R.A., Pinto, L.H., 2002. The gate of the influenza virus M$_2$ proton channel is formed by a single tryptophan residue. J. Biol. Chem. 277, 39880–39886. https://doi.org/10.1074/jbc.M206582200.

Tataridis, D., Fytas, G., Kolocouris, A., Fytas, C., Kolocouris, N., Foscolos, G.B., Padalko, E., Neyts, J., De Clercq, E., 2007. Influence of an additional 2-amino substituent of the 1-aminoethyl pharmacophore group on the potency of rimantadine against influenza virus. A. Bioorg. Med. Chem. Lett. 17, 692–696. https://doi.org/10.1016/j.bmcl.2006.10.092.

Thiel, G., Baumeister, D., Schroeder, I., Kast, S.M., Van Etten, J.L., Moroni, A., 2011. Minimal art: or why small viral K+ channels are good tools for understanding basic structure and function relations. Biochim. Biophys. Acta Biomembr. 1808, 580–588. https://doi.org/10.1016/j.bbamem.2010.04.008.

Thomaston, J.L., DeGrado, W.F., 2016. Crystal structure of the drug-resistant S31N influenza M2 proton channel. Protein Sci. 25, 1551–1554. https://doi.org/10.1002/pro.2937.

Thomaston, J.L., Konstantinidi, A., Liu, L., Lambrinidis, G., Tan, J., Caffrey, M., Wang, J., Degrado, W.F., Kolocouris, A., 2020. X-ray crystal structures of the influenza M2 proton channel drug-resistant V27A mutant bound to a spiro-adamantyl amine inhibitor reveal the mechanism of adamantane resistance. Biochemistry acs.biochem.9b00971. https://doi.org/10.1021/acs.biochem.9b00971.

Thomaston, J.L., Nguyen, P.A., Brown, E.C., Upshur, M.A., Wang, J., DeGrado, W.F., Howard, K.P., 2013. Detection of drug-induced conformational change of a transmembrane protein in lipid bilayers using site-directed spin labeling. Protein Sci. 22, 65–73. https://doi.org/10.1002/pro.2186.

Thomaston, J.L., Polizzi, N.F., Konstantinidi, A., Wang, J., Kolocouris, A., DeGrado, W.F., 2018. Inhibitors of the M2 proton channel engage and disrupt transmembrane networks of hydrogen-bonded waters. J. Am. Chem. Soc. 140, 15219–15226. https://doi.org/10.1021/jacs.8b06741.

Thomaston, J.L., Woldeyes, R.A., Nakane, T., Yamashita, A., Tanaka, T., Koiwai, K., Brewster, A.S., Barad, B.A., Chen, Y., Lemmin, T., Uervirojnangkoorn, M., Arima, T., Kobayashi, J., Masuda, T., Suzuki, M., Sugahara, M., Sauter, N.K., Tanaka, R., Nureki, O., Tono, K., Joti, Y., Nango, E., Iwata, S., Yumoto, F., Fraser, J.S., DeGrado, W.F., 2017. XFEL structures of the influenza M2 proton channel: room temperature water networks and insights into proton conduction. Proc. Natl. Acad. Sci. U.S.A. 114, 13357–13362. https://doi.org/10.1073/pnas.1705624114.

Thomaston, J.L., Wu, Y., Polizzi, N., Liu, L., Wang, J., DeGrado, W.F., 2019. X-Ray crystal structure of the influenza A M2 proton channel S31N mutant in two conformational states: an open and shut case. J. Am. Chem. Soc. 141, 11481–11488. https://doi.org/10.1021/jacs.9b02196.

Tietjen, I., Ntie-Kang, F., Mwimanzi, P., Onguéné, P.A., Scull, M.A., Idowu, T.O., Ogundaini, A.O., Meva'a, L.M., Abegaz, B.M., Rice, C.M., Andrae-Marobela, K., Brockman, M.A., Brumme, Z.L., Fedida, D., 2015. Screening of the pan-african natural product library identifies ixoratannin A-2 and boldine as novel HIV-1 inhibitors. PLoS One 10, e0121099. https://doi.org/10.1371/journal.pone.0121099.

To, J., Torres, J., 2019. Viroporins in the influenza virus. Cells 8, 654. https://doi.org/10.3390/cells8070654.

Tokuriki, N., Oldfield, C.J., Uversky, V.N., Berezovsky, I.N., Tawfik, D.S., 2009. Do viral proteins possess unique biophysical features? Trends Biochem. Sci. 34, 53–59. https://doi.org/10.1016/j.tibs.2008.10.009.

Tu, Q., Pinto, L.H., Luo, G., Shaughnessy, M.A., Mullaney, D., Kurtz, S., Krystal, M., Lamb, R.A., 1996. Characterization of inhibition of M2 ion channel activity by BL-1743, an inhibitor of influenza A virus. J. Virol. 70, 4246–4252.

Venkatraman, S., Njoroge, F.G., Girijavallabhan, V.M., Madison, V.S., Yao, N.H., Prongay, A.J., Butkiewicz, N., Pichardo, J., 2005. Design and Synthesis of Depeptidized 5088–5091.

Wang, C., Lamb, R.A., Pinto, L.H., 1995. Activation of the M2 ion channel of influenza virus: a role for the transmembrane domain histidine residue. Biophys. J. 69, 1363–1371. https://doi.org/10.1016/S0006-3495(95)80003-2.

Wang, C., Takeuchi, K., Pinto, L.H., Lamb, R.A., 1993. Ion channel activity of influenza A virus M2 protein: characterization of the amantadine block. J. Virol. 67, 5585–5594.

Wang, J., Cady, S.D., Balannik, V., Pinto, L.H., DeGrado, W.F., Hong, M., 2009. Discovery of spiro-piperidine inhibitors and their modulation of the dynamics of the M2 proton channel from influenza A virus. J. Am. Chem. Soc. 131, 8066–8076. https://doi.org/10.1021/ja900063s.

Wang, J., Li, F., Ma, C., 2015. Recent progress in designing inhibitors that target the drug-resistant M2 proton channels from the influenza a viruses. Biopolymers 104, 291–309. https://doi.org/10.1002/bip.22623.

Wang, J., Ma, C., Fiorin, G., Carnevale, V., Wang, T., Hu, F., Lamb, R.A., Pinto, L.H., Hong, M., Klein, M.L., Degrado, W.F., 2011a. Molecular dynamics simulation directed rational design of inhibitors targeting drug-resistant mutants of influenza A virus M2. J. Am. Chem. Soc. 133, 12834–12841. https://doi.org/10.1021/ja204969m.

Wang, J., Ma, C., Wu, Y., Lamb, R.A., Pinto, L.H., DeGrado, W.F., 2011b. Exploring organosilane amines as potent inhibitors and structural probes of influenza A virus M2 proton channel. J. Am. Chem. Soc. 133, 13844–13847. https://doi.org/10.1021/ja2050666.

Wang, J., Qiu, J.X., Soto, C., Degrado, W.F., 2011c. Structural and dynamic mechanisms for the function and inhibition of the M2 proton channel from influenza A virus. Curr. Opin. Struct. Biol. https://doi.org/10.1016/j.sbi.2010.12.002.

Wang, Jun, Wu, Y., Ma, C., Fiorin, G., Wang, Jizhou, Pinto, L.H., Lamb, R.A., Klein, M.L., DeGrado, W.F., 2013a. Structure and inhibition of the drug-resistant S31N mutant of the M2 ion channel of influenza A virus. Proc. Natl. Acad. Sci. U.S.A. 110, 1315–1320. https://doi.org/10.1073/pnas.1216526110.

Wang, Jizhou, Ma, C., Wang, Jun, Jo, H., Canturk, B., Fiorin, G., Pinto, L.H., Lamb, R.A., Klein, M.L., DeGrado, W.F., 2013b. Discovery of novel dual inhibitors of the wild-type and the most prevalent drug-resistant mutant, S31N, of the M2 proton channel from influenza A virus. J. Med. Chem. 56, 2804–2812. https://doi.org/10.1021/jm301538e.

Wang, Y., Hu, Y., Xu, S., Zhang, Y., Musharrafieh, R., Hau, R.K., Ma, C., Wang, J., 2018. In vitro pharmacokinetic optimizations of AM2-S31N channel blockers led to the discovery of slow-binding inhibitors with potent antiviral activity against drug-resistant influenza A viruses. J. Med. Chem. 61, 1074–1085. https://doi.org/10.1021/acs.jmedchem.7b01536.

Watkins, L.C., Liang, R., Swanson, J.M.J., Degrado, W.F., Voth, G.A., 2019. Proton induced conformational and hydration dynamics in the influenza A M2 channel HHS public access. J. Am. Chem. Soc. 141, 11667–11676. https://doi.org/10.1021/jacs.9b05136.

Wingfield, W.L., Pollack, D., Grunert, R.R., 1969. Therapeutic efficacy of amantadine HCl and rimantadine HCl in naturally occurring influenza A2 respiratory illness in man. N. Engl. J. Med. 281, 579–584. https://doi.org/10.1056/NEJM196909112811102.

Wright, A.K., Batsomboon, P., Dai, J., Hung, I., Zhou, H.-X., Dudley, G.B., Cross, T.A., 2016. Differential binding of rimantadine enantiomers to influenza A M2 proton channel. J. Am. Chem. Soc. 138, 1506–1509. https://doi.org/10.1021/jacs.5b13129.

Wu, Y., Canturk, B., Jo, H., Ma, C., Gianti, E., Klein, M.L., Pinto, L.H., Lamb, R.A., Fiorin, G., Wang, J., Degrado, W.F., 2014. Flipping in the pore: discovery of dual inhibitors that bind in different orientations to the wild-type versus the amantadine-resistant s31n mutant of the influenza a virus m2 proton channel. J. Am. Chem. Soc. 136, 17987–17995. https://doi.org/10.1021/ja508461m.

Zhao, X., Jie, Y., Rosenberg, M.R., Wan, J., Zeng, S., Cui, W., Xiao, Y., Li, Z., Tu, Z., Casarotto, M.G., Hu, W., 2012. Design and synthesis of pinanamine derivatives as anti-influenza A M2 ion channel inhibitors. Antivir. Res. 96, 91–99. https://doi.org/10.1016/j.antiviral.2012.09.001.

Zhou, H.X., Cross, T.A., 2013. Modeling the membrane environment has implications for membrane protein structure and function: influenza A M2 protein. Protein Sci. https://doi.org/10.1002/pro.2232.